Modelling Subglacial Hydrology under Future Climate Scenarios in Wilkes Subglacial Basin, Antarctica

by

Kevin Siu

A thesis
presented to the University of Waterloo
in fulfillment of the
thesis requirement for the degree of
Masters of Mathematics
in
Applied Mathematics

Waterloo, Ontario, Canada, 2022

Author's Declaration

I hereby declare that I am the sole author of this thesis. This is a true copy of the thesis, including any required final revisions, as accepted by my examiners.

I understand that my thesis may be made electronically available to the public.

Abstract

The Greenland and Antarctic ice sheets have differing climates, which makes surface melt a significant hydrological source in Greenland but not currently in Antarctica. Due to a changing climate and warming air temperatures, Antarctica is predicted to experience more surface meltwater in the future. This will likely lead to surface features common in Greenland today, such as supraglacial lakes and moulins, to also form over grounded ice in Antarctica. Moulins in particular are important because they will route this surface melt into basal drainage networks. The resulting change in subglacial drainage characteristics and water volumes will potentially have far-reaching impacts on ice dynamics, ice shelf melt, grounding line stability, and ultimately global sea level rise. To examine this, we model the hydrological system in Wilkes Subglacial Basin, East Antarctica using estimations of the future climate to incorporate moulins and surface melt. We use predictive data generated by the Community Climate System Model 4 (CCSM4) for surface runoff in Antarctica for the year 2100 as inputs to the Glacier Drainage System (GlaDS) subglacial hydrology model. We compare the modelling results from two different Representative Concentration Pathway (RCP) scenarios, RCP 2.6 and RCP 8.5. Moulin locations are predicted using current strain rates along preferential surface hydrology flow pathways and we also compare modelling results with different numbers and locations of moulins. We find that an increase in surface water input from none to RCP 2.6 to RCP 8.5 has a larger impact on basal drainage rates, channel extent, and water pressure near the grounding line. However, compared to increasing surface water inputs, we also find that increasing the number and extent of moulins can have an even larger impact on the subglacial hydrology system. This shows that both moulin formation and the evolution of the climate will play a role in the development of the subglacial hydrology system, which will be important for future ice flow speeds and ice shelf melt rates near the grounding line.

Acknowledgements

I would like to thank Dr. Christine Dow for all the knowledge and opportunities she has provided me over the years. Her dedication has meant a lot to me, and I'm lucky to have someone like her to look up to. I would also like to acknowledge my parents and brother for being the meaningful constant in my life. Lastly, my gratitude goes out to all my amazing friends for the experiences and memories that define so much of my existence.

Table of Contents

List of Figures

List of Tables

Chapter 1

Introduction

Humans have now changed the composition of the atmosphere to the point of significantly affecting the climate around the world. Furthermore, the energy production, transportation, and agriculture that defines the modern lifestyle still emits significant amounts of greenhouse gases (Ritchie et al., 2020; Ge et al., 2020). Decisions and actions to aim for net-zero greenhouse gas emissions in the coming decades will be critical in changing climate outlooks for the rest of this century and beyond. Without action, the worst consequences we may face include more extreme weather events, increasing ocean acidification, and rising sea levels. However, even under the best case scenarios that reach net-zero soon, sea levels are still projected to continue rising until the year 2300 due to the delayed response that previously emitted greenhouse gases have on sea levels (Mengel et al., 2018).

A rising sea level affects coastal communities around the world by pushing coastlines inland and increasing the risk of extreme flooding. One main contributor to rising sea levels is thermal expansion from increasing ocean temperatures, which increases the volume of the ocean even without any addition of water. The other main contributor to rising sea levels is grounded ice when it is transferred to the oceans either by flotation or melting (Oppenheimer et al., 2019). This makes the study of the world's ice—also known as the cryosphere—important to understanding how sea levels will continue to rise in the future. The main aim of this thesis is to use climate modelling data along with subglacial hydrology modelling to examine the evolution of subglacial hydrology and the role it could play in the future of the Antarctic ice sheet. To introduce this topic, we begin by covering the basics of glaciology and the differences between glaciers and ice sheets in Section 1.1. Covered next in Section 1.2 is the basics of how water flows through a glacier, also known as glacial hydrology. Finally, Section 1.3 includes a description of the specific region in Antarctica that is modelled, the Wilkes Subglacial Basin in East Antarctica.

1.1 Temperate Glaciers and Ice Sheets

Glaciers are large ice masses that are formed when a region has a long, consistent history of positive annual mass balances. The mass balance of a glacier is the sum between all

processes that add (accumulate) or subtract (ablate) from the ice mass. A positive mass balance means that accumulation, typically from precipitation, must outweigh ablation, typically from melt and runoff, or calving of the ice front. However, the definition of a glacier also requires that the glacier must move under its own weight. This is typically fullfilled automatically when an ice mass becomes large enough because its own weight either creates large stresses that cause internal deformation and/or overcomes basal friction and causes bulk sliding and scraping of the underlying terrain. Two regions on Earth with climatic conditions that are cold enough for glacier formation are high altitude mountains and the polar regions.

High altitude mountains support glacier growth as higher altitudes lower air temperatures and decrease ablation. As a mountain or alpine glacier forms at high altitudes, its own natural motion downhill can bring it to lower altitudes where ablation begins to exceed accumulation. This lets us define the altitude at which a glacier experiences balanced accumulation and ablation, which is called the equilibrium line altitude (ELA). These glaciers are sensitive to climate change as warmer temperatures move the ELA higher, causing a glacier to melt and retreat up the mountain (Benn & Evans, 2013). Retreating glaciers contribute to sea level rise when the meltwater they produce reach the ocean via watersheds. Although the alpine glacier contribution to sea level rise has been the dominant source in the last century (Oppenheimer et al., 2019), the vast majority of land ice and a concerning contributor to sea level rise by the end of this century and beyond comes from Antarctica (Morlighem et al., 2020) and Greenland (Mouginot et al., 2019).

The polar regions promote glacier growth as latitudes closer to the poles experience colder temperatures. Each of the poles has an ice mass that is large enough to classify them as ice sheets instead of glaciers. Ice sheets are important contributors to sea level rise due to the sheer volume of freshwater they keep from entering the ocean. The southern polar region contains the largest ice sheet in the world, which spans the majority of the continent of Antarctica. In the north, the Arctic ocean dominates the area all around the pole, but it still has the second largest ice sheet which is on the island of Greenland. The motion of both ice sheets (as well as other ocean-terminating glaciers) cause ice to flow into the ocean, where the resulting floating section (as ice is less dense than water) is then called an ice shelf. Floating ice shelves perform an important role called buttressing, which slows down the motion of grounded ice from entering the ocean, which is a main way ice sheets increase sea levels. Buttressing is strongest when ice shelves are pinned onto ocean floor features or are enclosed by land in a fjord (Fürst et al., 2016). However, ice shelves can also be subject to additional melting from the ocean. The boundary between floating ice shelves and the grounded ice sheet is where land, sea, and the overlying ice all meet and is called the grounding line. This boundary can move over time, which can affect where the ice shelf begins to float and how far inland ocean water can reach. Overall, the ice sheets of the polar regions are sensitive to climate change when ice shelves thin and collapse which removes buttressing, and when there is rapid grounding line retreat.

Even though the Antarctic and Greeland Ice Sheets are both formed in polar regions,

there is an important difference in their present day hydrology. On Greenland, there is widespread melting on the surface of the ice sheet (van den Broeke et al., 2016) during the summer melt season, which leads to a peak in surface runoff every year. In Antarctica, even during the austral summer, surface melting is still insignificant on most of the continent (Martín-Español et al., 2016), and is mostly limited to the Antarctic peninsula (Trusel et al., 2013). The main reason for this difference is that air temperatures over Greenland have increased enough over the past 30 years for surface melt to now become a significant ablation component on the ice sheet (Mouginot et al., 2019). Although Antarctica is not at this point yet, climate modelling has predicted that under continued warming and climate change we will start to see surface melt become the main hydrological source in Antarctica by the end of this century (Barthel et al., 2020).

The most obvious consequence of surface melting on ice sheets is that if runoff eventually drains into the oceans (instead of being retained for example in firn aquifers or refreezing), it will directly contribute to sea level rise. However, the existence of meltwater on ice sheets has many other complex consequences like increasing the albedo of the ice sheet surface (Tedesco et al., 2012), or driving surface crevasses all the way to the bottom of the ice sheet in a process called hydrofracturing (Das et al., 2008). The focus of my research is another such consequence of surface meltwater, namely once it reaches the base of the ice sheet, how it can affect the ice-bed interface which affects an ice sheet's overall motion and dynamics.

1.2 Glacial Hydrology

Glacial hydrology is divided into three subdomains based on the location of water in and around the ice (Fountain & Walder, 1998). Supraglacial hydrology covers water flowing on top of the glacier between the ice and the atmosphere. This includes water that can be captured and stored in firn aquifers (Chu et al., 2018). The firn layer on top of a glacier is snow that has fallen and is in the process of being compressed, but has not yet become the generally impermeable, solid ice that makes up the bulk of the glacier (Cuffey & Paterson, 2010). Another mode of supraglacial hydrology are river systems that can form on the ice like on ground, however, they can also flow into crevasses or moulins (open, vertical shafts in a glacier) which brings the water into the main body of the ice. Englacial hydrology covers water flowing inside the ice, where lateral channels can transport water horizontally, or water can be transported vertically from the supraglacial level all the way to the base of the glacier, known as the subglacial level. My research in modelling subglacial hydrology is concerned with how water introduced into the base of a glacier drains and where it will eventually exit at a terminus over the grounding line.

Even though there is a large mass of ice above the subglacial level, water can still drain and form the equivalent of lake and river systems. In general there are two main drainage types that subglacial hydrology systems can exist in (Fountain & Walder, 1998). Distributed, inefficient drainage systems are characterized by complicated flow paths underneath the

ice that water is routed through. A typical example of this is a linked cavity system where water flows in cavities formed by the ice flowing over an uneven bed topography (Iken & Bindschadler, 1986). These cavities can link with one another, but the path for water flow will be circuitous through the bed topography, which makes overall drainage through cavities inefficient. This inefficiency can cause water to build up in the distributed drainage system when water is introduced faster than it can drain, which can increase water pressure. This is important because then the water can provide an upwards force on the overlying ice, reducing friction between the ice and ground and facilitating faster glacier motion (Iken & Bindschadler, 1986). The second subglacial drainage type is called channelized, or efficient drainage systems, which are the subglacial equivalent of subaerial river systems. Channels can form not only by carving into the ground underneath, known as Nye (N-)channels, but also by melting into the ice above, known as Röthlisberger (R-)channels (Röthlisberger, 1972). Channels provide a faster and more direct means for water to flow through the subglacial system. These two drainage modes for subglacial hydrology are important to how the Glacier Drainage System (GlaDS) numerical model is implemented (Werder et al., 2013), and will be discussed in more detail in Section 3.1.

Once water is routed through a subglacial hydrology system, where and how it exits the glacier can be important to consider. For some land terminating glaciers, there can be sudden outburst flooding when meltwater is built up only to be released all at once. This can be disastrous for anything downstream as rivers and streams overflow rapidly (Benn & Evans, 2013). For Antarctic glaciers, consistent, localized subglacial outlet flow can affect the floating ice shelf. Having significant channelization in the subglacial hydrology system can lead to highly localized flow coming out through the grounding line (Le Brocq et al., 2013). This subglacial discharge can then initiate circulation that brings deep, warm water from the Southern Ocean known as Circumpolar Deep Water (CDW) up to convect and locally melt the underside of the ice shelf (Wei et al., 2020). This sub ice shelf melting can then weaken the buttressing effect (Alley et al., 2016), causing acceleration of grounded ice towards the ocean, accelerating rising sea levels (Fürst et al., 2016).

These examples show the complexity that can be found in trying to understand the physical processes of glaciers. This project contributes to predicting the future of the Antarctic ice sheet by modelling its subglacial hydrology. I focus on modelling a region in Antarctica as the Antarctic Ice Sheet is expected to undergo changes due to warming air and ocean temperatures this century.

1.3 Wilkes Subglacial Basin, East Antarctica

A continent-wide model of Antarctica was ruled out based on the overall size of the continent, computational limitations, and a desired mesh resolution. As a result, various regions in Antarctica were considered instead, including regions near Amery ice shelf, Thwaites glacier, and the Filchner-Ronne ice shelf. The Wilkes Subglacial Basin was ultimately chosen after an analysis comparing climate model outputs, subglacial melt rates,

and overall area of the various regions.

The Wilkes Subglacial Basin is a region in East Antarctica defined as a collection of subglacial drainage basins that will be a useful delineation for applying boundary conditions in subglacial hydrology modelling (further discussed in Section 3.3). Heading north from the region, the Wilkes Subglacial Basin faces in the general direction of Australia and New Zealand. Figure 1.1 shows the position of the region in the polar stereographic projection of Antarctica, with the origin of the coordinate system being the geographic south pole. Notable named outlet glaciers are labelled in Figure 1.1b. From right to left, they include Mertz Glacier, Ninnis Glacier, Cook Ice Shelf, Matusevich Glacier, Rennick Glacier, and Lillie Glacier. Cook Ice Shelf is attached to two glaciers called Cook East and Cook West.

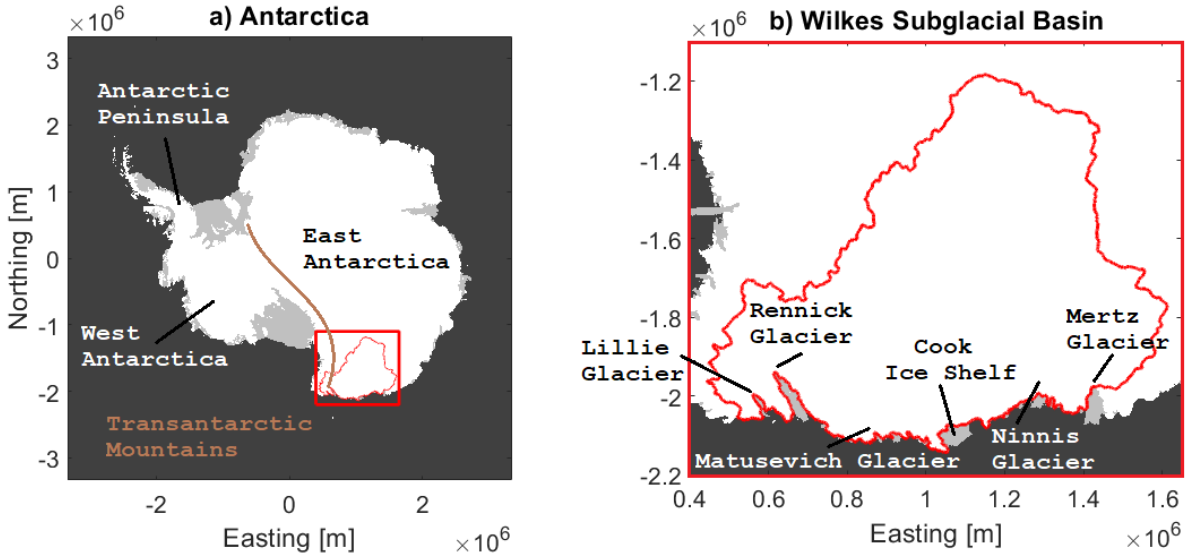

Figure 1.1: Location of Wilkes Subglacial Basin in Antarctica. Background colours denote grounded ice (white), floating ice (light grey), and ocean (dark grey) from BedMachine Antarctica (Morlighem et al., 2020). a) Map of Antarctica with the zoom-in region boxed in red. Major regions of Antarctica are labelled along with the Transantarctic Mountains (brown) which divides Antarctica into east and west. b) Zoomed-in region of Antarctica with the model domain outlined in red. The glaciers in the region are individually named.

The rest of the thesis starts with Chapter 2 and a review of literature covering early work in glacial hydrology up to today, and the development of subglacial hydrology modelling. Chapter 3 then further describes the project including the GlaDS model and a new moulin positioning algorithm used alongside climate model predictions to create different future scenarios. Chapter 4 contains the results of the modelling, followed by a discussion in Chapter 5, which finally leads to the conclusion in Chapter 6.

Chapter 2

Literature Review

2.1 Summary of the Literature

We start the literature review by summarizing past work relevant to subglacial hydrology modelling. Research conducted during the beginning of the study of glacial hydrology use valley glaciers (alpine glaciers within a valley) as the primary physical model of a glacier. We then look at the development of a theoretical framework for glacial hydrology trying to explain how glaciers in the past formed some perplexing geographical features that can still be seen today. Next, we discuss the history of glacial hydrology modelling and the work done to be able to compare outputs from different models. In the next section, we discuss what the literature summary means for Antarctica and work trying to model subglacial hydrology there.

2.1.1 Foundational Ideas and Methods in the Study of Valley Glaciers

Shreve (1972) produced theoretical models of water flow through a temperate glacier, relevant parameters for passage creation, and also provided physical evidence for it. Beginning by comparing temperate glaciers to karst regions, water flowing on the surface can be captured by openings that redirect it to flow underground, or under ice. This provided a visualization for the three mode breakdown of glacial hydrology: supraglacial hydrology with water flowing on top of glaciers, englacial hydrology which covers water passing through passages in the ice, and subglacial hydrology which covers water flowing between the ice and ground underneath. An important consideration in the theoretical model of glacial hydrology is that while water passes through a glacier, it affects the passages it uses through phase changes and ice deformation.

To determine how water flows, it is assumed to always be down the gradient of hydraulic potential, Φ, which is defined to be

$$\Phi = \Phi_0 + p_w + \rho_w g z, \tag{2.1}$$

where Φ_0 is an arbitrary constant, p_w is water pressure inside an ice-walled passage, and the right hand term is the gravitational potential which depends on the water density, ρ_w, gravitational constant, g, and elevation, z. While the last term is similar to hydrostatic pressure in a water column, which increases with depth, this gravitational potential is meant to decrease as water flows down elevation. This equation makes the assumption that water everywhere in a glacier can be treated as if it were in a water-filled passage, which allows for varying, dynamic passageways to be accounted for. It also makes it so that water is assumed to flow down elevation except into high water pressure regions controlled by ice overburden pressure and changes in the size of the passages. These varying passageways balance overburden pressure and water pressure, and are affected by the effective strain-rate of ice. Overburden pressure is the weight of ice above the passage, and the effective strain-rate of ice is related to the shear stress and subsequent deformation of ice walls. This is how Shreve describes passage dynamics, which are based on assumptions of a steady state system where inputs to the glacier's hydrological system do not vary temporally. Geographical evidence is then used to support the importance and impact of water flowing through a glacier. Shreve points to features like long, sinuous ridges called eskers and tunnel valleys left behind by glaciers that have passed through currently unglaciated regions. The formation of these features rely on the existence of subglacial hydrological systems of past glaciers.

Iken (1981) used another method besides theoretical considerations and geographical evidence, which is a computational model to try and determine how a subglacial water system affects a glacier's overall sliding velocity. This was done to try and understand observations that temperate glacier velocities can change rapidly over short time periods of days or hours, and whether the drainage dynamics in the subglacial hydrology system could account for them. A two dimensional finite element model was used, with a simplified sloped sinusoidal geometry, shown in Figure 2.1. The model outputs linked fluctuating water input to unstable changes in the linked cavity system and even further to changing sliding velocities. This showed that a changing subglacial hydrology system could account for overall glacier velocity fluctuations. However, many simplifications were made to be able to use simplified theoretical results, including smooth glacier beds, a constant bed incline, and only considering normal stresses along a bump. Even more important is the simplification to only consider cavities of the distributed, inefficient drainage system, instead of including channels. However, all these simplifications were pointed out, with the call for more realistic assumptions and future work to be able to state more conclusively the link between glacial hydrology and ice dynamics.

Another method for studying glaciers is collecting in-situ data as showcased in Iken & Bindschadler (1986). They collected data on Findelengletscher in Switzerland during the melt season of 1982 to try and detect diurnal velocity cycles. If these velocity cycles could then be connected with diurnal meltwater cycles then a glacier's motion could be correlated to the melt water being produced on it. Angles and distances between various points on the glacier were collected to determine sliding velocities. Boreholes were drilled to determine subglacial water pressure and connectivity of the channelized drainage system. Efficiency of

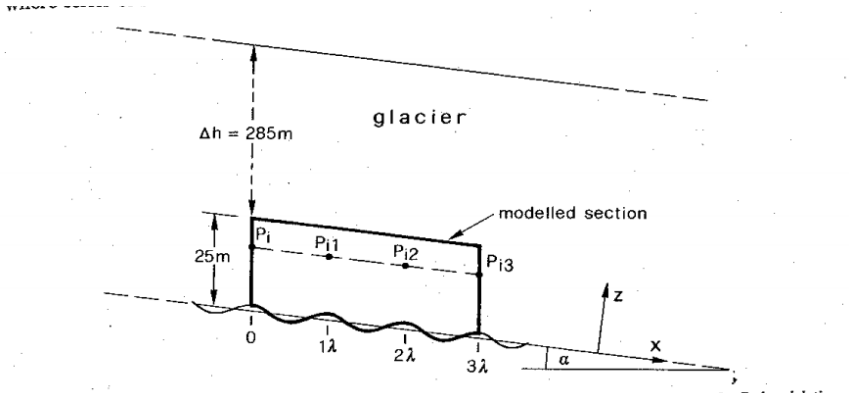

Fig. 2. Modelled section at the bottom of a glacier. Surface slope and mean bed slope of the glacier is α = 4°. Bed undulations have a period of λ = 20 m.

Figure 2.1: Schematic of an early subglacial hydrology model. The model used an idealized geometry of a glacier bed with a constant slope and sinusoidal bed topography. The physical parameters are based on the Unteraargletscher located in the Swiss Alps. From Iken (1981).

the drainage system was determined from dye tracing experiments. All of this information was then synthesized to compare with theoretical and computational predictions.

One of the comparisons made was the empirically measured versus theoretically computed relationship between subglacial water pressure and sliding velocity. Theoretically, sliding velocities should increase along with water pressure starting at a lower pressure threshold known as the separation pressure (when there is enough pressure to start creating separation between ice and bed, reducing friction). The sliding velocity is then predicted to become unstable past a higher threshold called the critical pressure. While the general relationship of increasing velocity while water pressure increases was confirmed, when the theoretical curve was matched to the separation pressure, it predicted an extremely low critical pressure. This meant the theory predicts unstable sliding at pressures where a normal sliding relationship was observed, revealing a limitation of the idealized theoretical relationship. Oversimplifications that could explain the low predicted critical pressure included: the idealistic sinusoidal bed topography, the assumption of impermeable, undeformable bed, and no friction from a perfectly lubricated bed.

Another important finding from the measurements made on Findelengletscher is that it did not appear to form an efficient, channelized system during the melt season. They did not observe the pattern of decreases in water pressure associated with the development of a subglacial channel that draws in water from its surrounding inefficient cavity system. The reasons given for this was that Findelengletscher had both a low discharge rate into the subglacial hydrology system and a fast basal velocity that would close any channels that may form.

2.1.2 Advancements in Theoretical Models of Glacial Hydrology

Walder & Fowler (1994) set out to challenge the simplifying assumption that glacier beds are rigid, unmoving, and impermeable. Using theoretical considerations and analysis, they created a new model for subglacial hydrology systems where the hard bed is swapped with a deformable and porous sediment layer called till, which is in turn laid over a hard bed. The addition of this till layer to the makeup of the bed allows for more forms of glacier flow, as the till itself can shear and move, bringing along the ice above it. This also allows for a more complex subglacial hydrology system as in addition to both channels (formed by cutting up into the ice as Röthlisberger (R-) channels) and thin water films, there can be channels cut into the till called canals. The theoretical modelling shows R-channels and canals occupying different regimes of effective pressure, where above some characteristic pressure only R-channels are stably formed and below the characteristic pressure, only canals are stable. These theoretical considerations which add nuance to the previous idealistic assumptions about factors that affect subglacial hydrology and ice dynamics are important as more evidence suggests a more complex coupling between hydrology and ice dynamics, especially for understanding the differences between ice sheets and valley glaciers.

Fountain & Walder (1998) summarized the breakdown of hydrology through temperate glaciers into supra-, en-, and subglacial hydrology. It included discussion of the role firn aquifers play in collecting and storing supraglacial water to smooth out otherwise abrupt changes in water input further down in the englacial hydrological system. It also describes distributed and channelized subglacial hydrological systems as slow and fast drainage systems respectively, which can dynamically switch or coexist underneath the same glacier. This shows one of the difficulties in modelling subglacial drainage systems, in that to do it properly both the distributed and channelized drainage systems of a glacier must be coupled together and simulated at the same time.

2.1.3 Hydrology Modelling

Creyts & Schoof (2009) described another way to model the distributed subglacial hydrology system, namely by having water flow in thin, macroporous sheets instead of the typical linked cavity system. The macroporous sheet comes from the idea that protrusions from the bed can be modelled as hemispherical sediment grains of varying radii and sizes, where for a given water film thickness only the largest sediment grains support the overlying ice. Water can then flow over smaller sediments as well as around the larger sediments that support the ice.

The thickness of the water film is constrained by stability in balancing the opposing forces increasing and decreasing the space between bed and ice. Opening of the space comes from viscous dissipation and pressure melting, while closing of the space comes from regelation and ice creep. This balance is calculated by a recursion scheme which looks

at different water thicknesses that correspond to support from different sediment sizes that spread and distribute overburden pressure. Results were found to allow for multiple stable water film thicknesses, which was interpreted as being analogous to the coupling between distributed and channelized drainage systems, where increasing from one stable film thickness to another increases the discharge rate like increasing the size and extent of subglacial channels.

Schoof (2010) also described another way to model subglacial hydrology, in the form of a system of connected subglacial conduits that incorporates both distributed and channelized drainage modes. A single conduit can be modelled from the balance of opening and closure rates. Rate of opening includes a linked cavity contribution from the sliding speed and a channel contribution from wall melting, while closure just considers viscous ice creep. Each individual conduit is found to have two stable configurations, which are denoted by a channel mode for the higher discharge rate and conduit cross-section and a cavity mode for the lower discharge rate and conduit cross-section. Modelling a whole subglacial system is then achieved by linking a large number of these individual conduits together. An important idea brought on by the results of this type of modelling on an ideal, synthetic domain, is that water input into a subglacial system has a nuanced effect on ice dynamics. The model showed that more water flow does not always mean faster glacier flow. Instead, velocities also depend on how and if a channelized drainage system forms and whether a critical rate of water flow is reached. For water flows above a critical rate, the model has the opposite relationship where increasing the water flow actually decreases ice flow. This is due to the nature of water draining through an R-channel being at a lower effective pressure than the same flow in a distributed, linked cavity system. If there is enough water flow to induce the formation of a channelized drainage system, this increase in input water can actually cause an overall decrease in effective pressure and therefore decrease sliding speed.

The subglacial drainage model used for my thesis is the Glacier Drainage System (GlaDS) model, first outlined in Werder et al. (2013). It is a two dimensional finite element model that simulates subglacial hydrology by coupling a distributed and a channelized drainage system together. The dynamic interplay between an inefficient and efficient drainage system is an important characteristic of subglacial hydrology systems (Fountain & Walder 1998, Shreve 1972). The model works on an unstructured triangular mesh, where each element is considered as a spatially averaged linked cavity, while each edge is considered as a conduit that can represent R-channels. The distributed and channelized drainage systems with their own domains can then be coupled together locally along the entire mesh which imitates the predicted coupling that is expected to take place underneath real glaciers. This stands in stark contrast to Creyts & Schoof (2009) which tries to take this dynamic into consideration with a single macroporous sheet system. However, a lot of inspiration was taken from Schoof (2010), in that both the distributed drainage system, and how channels are connected in the GlaDS model, are similar to how a single conduit operates in cavity mode, and how multiple conduits are connected, respectively. There is more details about the GlaDS model and how it is used in my project in Chapter 3.

2.1.4 Comparison Between Models

The GlaDS model has been compared to the plethora of other computational models created to simulate subglacial hydrology in Flowers (2015) and de Fleurian (2018). Flowers (2015) went over the basic theory of conservation laws and the different 'elements' of subglacial drainage to eventually build up the basis for all subglacial hydrology models. All the models are then split into three groups of models: groundwater hydrology models, next-generation models that add flow parameters to simulate unique subglacial hydrology characteristics, and multi-element drainage models like the GlaDS model which takes into account distributed and channelized drainage systems. This helps put into a historical perspective the progression of model complexity, sophistication, and applicability. This can then be used to see where future model development can come from, and what complexities could be added, like incorporating more drainage systems or a deformable bed, at what cost.

The Subglacial Hydrology Model Intercomparison Test Project (SHMIP) described in De Fleurian et al. (2018) also compared various subglacial hydrology models, however focused on directly comparing model outputs of effective pressure and subglacial discharge. So, only models that could produce these outputs were chosen. In addition, only models with linked cavity and R-channel based drainage systems were chosen (representing distributed and channelized systems respectively, where applicable). To ensure fair comparisons, each subglacial hydrology model were given the same set of synthetic scenarios, or suites, to run. A total of six different scenarios were designed with varying water input and topographies based on the different situations that glaciers face around the world. The results from comparing all the participating models was a general agreement between model outputs for simulated scenarios with low water input and slow variations in transient parameters. However, where the simpler models (that only include a distributed system) started disagreeing with the more complex, complete models (that also include a channelized drainage system like the GlaDS model), it is assumed the complex models are more accurate. In any case, the final arbiter for computational models is to be able to match real glacier data, and to be able to apply the model to make real world predictions with confidence.

2.2 Discussion

2.2.1 Why are we interested in the Antarctic?

While the valley glaciers located in mostly high altitude mountains were the primary subject of study in the past (Shreve 1972, Iken 1981), it is the two large ice sheets of Greenland and Antarctica that are the primary concerns for future sea level rise. As explained in Section 1.1, this is due to the fact that a majority of the grounded ice that has the potential to raise sea levels are found in Greenland and Antarctica.

Due to how remote, large, and thick the Antarctic Ice Sheet is, it was previously much harder to access and study Antarctic glaciers with traditional methods used on temperate glaciers. This means knowledge about the Antarctic ice sheet was a lot further behind than temperate glaciers, and big discoveries like in Le Brocq et al. (2013) were still being made fairly recently. Le Brocq et al. used remote sensing techniques to study features on Antarctic ice shelves that could indirectly point to the existence of a channelized drainage system underneath the grounded ice sheet and ice streams. After some features on Antarctic ice shelves were discovered in satellite imagery from the Moderate Resolution Imaging Spectroradiometer (MODIS), further airborne radar measurements were taken over these features which provided evidence for channels that appear underneath the floating ice shelves. These sub-ice-shelf channels might form as fresh meltwater is released over the grounding line from the subglacial hydrology system into the ocean, causing plumes that can bring warmer water to the base of the ice shelves. They may also be remnants of subglacial R-channels as grounded ice flows out to become floating ice shelves. This provides evidence that R-channels - and entire channelized drainage systems - do exist in the Antarctic, despite previous assumptions that only distributed drainage systems exist due to a lack of water input and shallow slopes at the bed.

2.2.2 Recent Work in Understanding Subglacial Hydrology

Being able to predict ice dynamics in Antarctica and Greenland will be important in predicting how sea levels will rise in the future. This means taking one step back to look at the significance of glacial hydrology to ice dynamics, which motivates a lot of new research into subglacial hydrology.

Werder (2016) looked at how overdeepenings in bed topography form, and how they impact subglacial hydrology. One of the hypotheses for the formation of overdeepenings states that the depth of an overdeepening stabilizes at a supercooling threshold where the bed slope is high enough to stop any channelized drainage system from operating or forming, and water is left to flow only through a distributed drainage system. A one dimensional R-channel model and the two dimensional GlaDS model (coupled R-channel system to a linked cavity system) were deployed to determine the supercooling threshold numerically. This also included a theoretical tweak to the previous supercooling threshold by taking into consideration an extra term for subglacial water pressure downstream from the overdeepening. Werder was then able to show that both models with the new threshold more accurately agreed with real data from overdeepenings in the Swiss Alps. This shows that using subglacial hydrological modelling as a tool, along with theory and real data, can help build more robust results.

Dow et al. (2018a) used the GlaDS model to study the subglacial lakes found in Recovery Ice Stream in East Antarctica. An important geographical feature of Recovery Ice Stream is the narrowing of the catchment which affects the subglacial hydrology by forcing all water in the system to build up to be able to flow through the narrowing. The modelling used

a time dependent surface elevation, while also running sensitivity tests covering different values of unknown parameters like channel and sheet conductivity to determine a range of possible model outputs. The model outputs were able to match up with the general areas of the subglacial lakes known from satellite altimetry, which is a confirmation that the GlaDS model is able to model the necessary subglacial hydrology characteristics that are required for subglacial lakes to form. Going even further, the model outputs also showed propagating transient pressure waves which are necessary for these subglacial lakes underneath an ice stream to fill, drain and even form in the first place. These could be analogous to the propagating pressure waves observed from direct borehole measurements in temperate glaciers that are caused by sudden increases in water input to the system (Iken & Bindshadler 1986). This application of a subglacial hydrology model shows that they can be used to predict features of Antarctic glaciers as well, even without surface water production or steep slopes in topography.

Poinar et al. (2019) took a look at the role firn aquifers play in changing how meltwater is introduced into the glacier and what effects it has on the overall subglacial drainage system. The GlaDS model was run using a synthetic model domain based on Helheim Glacier in Southeast Greenland, where firn aquifers are known to have an effect on supraglacial drainage. Different scenarios were then created with water inputs that varied both spatially and temporally to represent different states of the supraglacial drainage system. One of the ways the model outputs were analysed was to determine how a draining, upstream firn aquifer affects the subglacial hydrology downstream and elsewhere. One of the interesting results is that all scenarios with some upstream water input into the subglacial system showed the same effective pressure change as the one scenario where all water inputs are located at the downstream, lower elevations. By having even just 10% of total water input being released upstream via a firn aquifer, the effective pressure upstream increases while slightly decreasing downstream pressure. This shows the outsized effect firn aquifers can have on a subglacial drainage system by storing a relatively small percentage of meltwater instead of having it run directly through a moulin and into the subglacial drainage system.

Another recent study of the subglacial hydrology in Greenland was done by Cook et al. (2020) to try and fully model a tidewater glacier. To do this, three computational models were coupled together: the GlaDS model for subglacial hydrology, the Elmer/Ice model for ice flow and ice dynamics, and a one dimensional model that simulated submarine plumes at the calving front. The catchment and model domain was for Store Glacier in West Greenland, and three scenarios were modelled based on none, a low, and a high volume of surface melt entering the system representing a winter and two different summer conditions respectively. A result from the winter scenario shows that even without surface melt input into the subglacial hydrological system, the plume model was still able to drive convective plumes just based on geothermal and frictional heat sources generated within the glacier. Comparing the winter condition to the summer conditions with surface melt input, there was little change to the plume outputs which shows a weak correlation between surface inputs and plume melting. One reason for this would be the subglacial hydrology modelling modifying the temporal pattern of water inputs between surface inputs and

subglacial discharge outputs. This shows the importance of subglacial hydrology systems and in studying their downstream impacts.

Dow et al. (2020) is another example of an application of subglacial hydrology to try and learn more about Antarctic glaciers. With the focus being on Totten glacier in the Aurora Subglacial Basin (ASB) in East Antarctica, subglacial hydrology was modelled in this region using the GlaDS model. Another computational model called the Ice-sheet and Sea-level System Model (ISSM), was applied to find two necessary inputs for the GlaDS model, basal velocity and basal melt rate, from corresponding surface data of velocity, temperature, and mass balance along with a constant geothermal heat flux. Another input parameter which is the sheet conductivity was determined by matching distributed water thickness outputs of various conductivity parameters to specularity content data from radar measurements by the International Collaborative Exploration of the Cryosphere by Airborne Profiling (ICECAP). The results of the modelling provide predictions of subglacial hydrology parameters including channel locations, channel discharge rates, and effective pressure. This approach of using multiple methods alongside the GlaDS model provides a stronger foundation and justification for the model outputs, however it can still use real data to be able to fully validate the predictions.

These applications of subglacial hydrology theory and modelling, specifically the GlaDS model, enforce the fact that glacier features and behaviours are strongly influenced by how water moves through a glacier. These applications of modelling also show the importance of being able to corroborate numerical simulations with other methods like remote sensing data or theoretical considerations.

Chapter 3

Methods

This chapter will discuss how the modelling project was conducted. First, Section 3.1 will describe the GlaDS model used, split between looking at how the distributed drainage system is modelled, then the channelized drainage system (Werder et al., 2013). Section 3.2 will then cover all the datasets used to be able to specifically model the Wilkes Subglacial Basin. Section 3.3 will describe and look at the triangular mesh created for the model region to be run in GlaDS. Section 3.4 describes the algorithm developed for this project to calculate moulin locations based on the process of hydrofracturing. Finally, Section 3.5 describes the different scenarios performed in GlaDS from modelling the present day with no surface water input to all the different future scenarios with surface water input.

3.1 Glacier Drainage System (GlaDS) Model

I use the finite element Glacier Drainage System (GlaDS) model to simulate the subglacial hydrology system for this project. The following description of the GlaDS equations follows the paper first published by Werder et al. in 2013. The GlaDS model couples the mathematical descriptions of both a distributed and a channelized drainage system underneath a glacier. The goal of the model is to imitate the complex, dynamic interplay between the two drainage systems, which is a control on the motion of the overlying ice. It does this by assigning different domains on a triangular mesh to either system, namely mesh *elements* to the distributed system, labelled Ω_i, and mesh *edges* to the channelized system, labelled Γ_j.

3.1.1 Distributed Drainage System

The distributed drainage system in GlaDS is modelled after a system of linked cavities underneath a glacier. In each area corresponding to a mesh element, the size of the cavities and the tunnels connecting them are represented by the average water thickness, h. This is under the assumption that the linked cavity system is always full of water, so that the volume of water directly corresponds to the space in the linked cavities. The modelled

linked cavity system can enlarge, and thus hold more water, when the ice flows over bumps in the bed topography and melts cavities up into the ice. This is emulated by the opening rate of the linked cavity system, w, and is affected by the basal ice speed, u_b, and average bump height and spacing, h_r and l_r

$$w = \begin{cases} \frac{u_b(h_r - h)}{l_r} & \text{if } h < h_r \\ 0 & \text{otherwise.} \end{cases} \tag{3.1}$$

When the cavities are larger than the average bump height, the ice does not reach the bumps and so the rate of cavities opening reaches zero. The linked cavity system can also shrink due to viscous deformation of the overlying ice. How much the ice can flow to close the cavities depends on the effective pressure of the ice, N, equal to the difference in pressure of ice above, p_i, and water below, p_w:

$$N = \rho_i g H - p_w = p_i - p_w, \tag{3.2}$$

where ρ_i is the density of ice, g is the gravitational constant, and H is the ice thickness. This shows that the water below can play an extra role on the ice above it if it is pressurized. The closing rate, v, depends on the flow constants, $\tilde{A}$ and n:

$$v = \tilde{A} h |N|^{n-1} N. \tag{3.3}$$

The change in water thickness of the distributed linked cavity system is then

$$\frac{\partial h}{\partial t} = w - v. \tag{3.4}$$

This requires the water thickness to respond directly to how the cavities increase and decrease in size. Another way to think about the change in distributed water thickness is to consider the water itself and the conservation of mass. The water flowing in and out of a fixed region of the linked cavity system can be described by the water discharge, $\vec{q}$. This discharge is based on the subglacial hydraulic potential, ϕ:

$$\phi = \rho_w g B + p_w = \phi_m + p_w, \tag{3.5}$$

where ρ_w is the density of water and B is bed elevation. This is simply the sum between gravitational potential (how water flows in open rivers down terrain) and water pressure, equivalent to equation (2.1). Similar to Darcian flow (Benn & Evans, 2013), or flow through a porous medium, the water flowing through the linked cavity system is

$$\vec{q} = -k h^{\alpha} \left| \vec{\nabla} \phi \right|^{\beta - 2} \vec{\nabla} \phi, \tag{3.6}$$

where k is a constant known as the sheet conductivity, and α and β are empirical constants describing the type of flow. Water produced within the subglacial region, which corresponds to basal melt, can be described by a source term, m. This directs the sheet discharge down the gradient of hydraulic potential, while also being proportional to the amount of water

in the distributed drainage system. The conservation of mass then requires the continuity equation

$$\frac{\partial h}{\partial t} + \vec{\nabla} \cdot \vec{q} = m. \tag{3.7}$$

To be able to able to account for faster water storage in the linked cavity system, an additional englacial storage parameter, h_e, is included. This is proportional to the water pressure that holds water above the linked cavity system in englacial aquifers, and the englacial void ratio, e_v, which is the amount of space available in englacial aquifers

$$h_e = \frac{e_v p_w}{\rho_w g}. \tag{3.8}$$

Due to the proportionality to water pressure, this englacial storage parameter is able to respond to sudden influxes of water and corresponding increasing water pressure when opening cavities by sliding over bumps is too slow. The englacial storage parameter can also be seen as another source or sink in the distributed drainage system when water physically flows into englacial aquifers. So, this can add to the continuity equation to become

$$\frac{\partial h}{\partial t} + \frac{\partial h_e}{\partial t} + \vec{\nabla} \cdot \vec{q} = m, \tag{3.9}$$

and completes the mathematical implementation of the distributed drainage system in GlaDS.

3.1.2 Channelized Drainage System

The channelized drainage system in GlaDS is modelled after a spontaneous network of Röthlisberger channels (R-channels) forming due to high pressures in the distributed drainage system. High pressures allow for melting of ice above the subglacial drainage system in the direction of water flow to create R-channels. A network of R-channels then allows for the efficient drainage of water from the subglacial system by demand and along direct routes around the subglacial landscape. To be able to do this in GlaDS, channels are allowed to form on any of the edges in the mesh (except for the outside boundary edges, where boundary conditions are imposed). Each mesh edge is a discrete link that can possibly develop to be a part of a larger and longer R-channel, and is described by its own channel cross-sectional area, S. The rate of change is given by an opening and closing rate, similar to sheet thickness change in the distributed drainage system

$$\frac{\partial S}{\partial t} = \frac{\Xi - \Pi}{\rho_i L} - v_c \tag{3.10}$$

The opening rate of the ice in this case depends on the amount of ice that melts to make way for the R-channel. Assuming all ice to be at the pressure melting point, which also justifies the coexistence of both solid and liquid states of water in the first place, any heat energy added into the system converts a proportional mass of ice to liquid water by the latent heat of fusion, L. Ξ is the spatial and temporal rate of potential energy loss

Table 3.1: Summary of the parameters required for the distributed drainage system model in GlaDS.

Parameter	Variable	Value	Units
Sheet Water Thickness	h		m
Effective Pressure	N		Pa
Ice Overburden Pressure	p_i		Pa
Water Pressure	p_w		Pa
Time	t		s
Hydraulic Potential	ϕ		Pa
Bed Hydraulic Potential	ϕ_m		Pa
Cavity Opening Rate	w		m s^{-1}
Cavity Closing Rate	v		m s^{-1}
Sheet Discharge	$\vec{q}$		m^2 s^{-1}
Sheet Conductivity	k	5×10^{-4}	$m^{7/4}kg^{-1/2}$
Bedrock bump height	h_r	0.08	m
Cavity Spacing	l_r	2	m
Ice flow constant	$\tilde{A}$	2.5×10^{-25}	Pa^3s^{-1}
Glen's flow constant	n	3	
Englacial Void Ratio	e_v	1×10^{-5}	
Ice Density	ρ_i	910	kg m^{-3}
Gravitational Acceleration	g	9.8	m s^{-2}
Water Density	ρ_w	1000	kg m^{-3}
First Sheet Flow Exponent	α	5/4	
Second Sheet Flow Exponent	β	3/2	
Basal Sliding Speed	u_b	*	m s^{-1}
Ice Thickness	H	*	m
Bed Elevation	B	*	m
Sheet Source Term	m	*	m s^{-1}

*parameters that have a spatially variable dataset, described in Section 3.2

and dissipation in the channel, which depends on the discharge and change in hydraulic potential along the mesh edge, s

$$\Xi = \left| Q \frac{\partial \phi}{\partial s} \right| + \left| l_c q_c \frac{\partial \phi}{\partial s} \right| \tag{3.11}$$

The first term on the right hand side comes from the channel discharge, Q (defined further below), while the second term comes from the sheet discharge around the channel, q_c

$$q_c = -k h^{\alpha} \left| \frac{\partial \phi}{\partial s} \right|^{\beta-2} \frac{\partial \phi}{\partial s} \tag{3.12}$$

This second term is how water pressure in the distributed drainage system can affect - via the potential energy loss in the channel - the channel cross-sectional area of the channelized drainage system. Another way the distributed system is linked to the channelized system

is by changing the pressure melting point of the ice. Π is the rate of change of sensible heat, given by

$$\Pi = -c_t c_w \rho_w (Q + f l_c q_c) \frac{\partial p_w}{\partial s} \tag{3.13}$$

where c_t is the Clapeyron slope (defined here as the positive quantity), c_w is the specific heat capacity of water, and f is a factor that prevents freezing of a non-existent channel

$$f = \begin{cases} 1 & \text{if } S > 0 \text{ or } q_c \frac{\partial p_w}{\partial s} > 0 \\ 0 & \text{otherwise} \end{cases} \tag{3.14}$$

The closing rate of the channel, v_c, is similar to that for the sheet as both close due to pressure dependent viscous deformation

$$v_c = \tilde{A} S |N|^{n-1} N \tag{3.15}$$

where the constants $\tilde{A}$ and n are kept identical for lack of physical knowledge. Similar to the two-dimensional discharge for the distributed drainage system, the one-dimensional (in the direction of the mesh edge, s) discharge for the channelized drainage system, Q, is

$$Q = -k_c S^{\alpha_c} \left| \frac{\partial \phi}{\partial s} \right|^{\beta_c - 2} \frac{\partial \phi}{\partial s} \tag{3.16}$$

where k_c is the channel conductivity, and α_c and β_c are the channel versions of the flow constants describing sheet discharge in the distributed drainage system. This leads to the conservation of water mass for a single mesh edge

$$\frac{\partial S}{\partial t} + \frac{\partial Q}{\partial s} = \frac{\Xi - \Pi}{\rho_w L} + m_c \tag{3.17}$$

where now the first term on the right hand side is the amount of water gained (instead of ice lost) to open the channel, and m_c is the source term for water being introduced into the channel from the adjacent linked cavity system. This can be seen as a one-(spatial) dimensional version of Equation 3.7, where the rate of change of the channel cross-section along with the flux of (channel) discharge along an edge must balance any sources or sinks of water in the channel. Efficient channel drainage is known to poach water from the surrounding distributed drainage system as faster water flow and discharge decreases the pressure in the channel, creating a potential gradient directing surrounding water into the channel. This is the second way the distributed sheet system is coupled to the channel system after the energy rates Ξ and Π. The water source, m_c, is defined as

$$m_c = \vec{q} \cdot \vec{n}|_{\partial\Omega_{i_1}} + \vec{q} \cdot \vec{n}|_{\partial\Omega_{i_2}} \tag{3.18}$$

using the sheet discharge from the two adjacent elements and the direction normal to the edge.

Next, the channels are all coupled together via their intersections at the mesh nodes. The sum of all channel discharges attached to a node including external sources into the node, Q_m, must equal zero

$$\sum_j Q_j^k + Q_m^k = 0 \tag{3.19}$$

where k is the index for the specific node we are looking at, and j indexes all channels (mesh edges) attached to the k^{th} node. The external source attached to the nodes is where surface input directed into moulins is added. This means any moulin inputs from the surface will be directly applied to the channelized drainage system and not the distributed drainage system, which is required for model stability.

To solve using finite elements, the differential equations for the hydraulic potential, ϕ, are multiplied by a test function and then integrated over both mesh elements Ω_i and edges Γ_j to turn into a weak form (Werder et al., 2013). Time stepping is then done using MATLAB's ode15s stiff differential equation solver in first order, and all the code is written in MATLAB. Also solved are the evolution equations for the sheet thickness, h, and channel cross-section, S, Equations 3.4 and 3.10 respectively. This completes the description of the GlaDS model, and next we will look at the data used to be able to set model parameters to describe the Wilkes Subglacial Basin.

Table 3.2: Summary of the additional parameters required for the channelized drainage system model in GlaDS.

Parameter	Variable	Value	Units
Channel Cross-Sectional Area	S		m^2
Channel Discharge	Q		$\mathrm{m}^3\ \mathrm{s}^{-1}$
Along Edge Distance	s		m
Channel Press-Melt	Ξ		$\mathrm{W\ m}^{-1}$
Sheet Flow Beneath Channel	q_c		$\mathrm{m}^2\ \mathrm{s}^{-1}$
Channel Dissipation	Π		$\mathrm{W\ m}^{-1}$
Channel Freezing Factor	f		
Channel Closing Rate	v_c		$\mathrm{m}^2\ \mathrm{s}^{-1}$
Channel Input from Sheet	m_c		$\mathrm{m}^2\ \mathrm{s}^{-1}$
Channel Conductivity	k_c	5×10^{-2}	$\mathrm{m}^{3/2}\mathrm{kg}^{-1/2}$
Sheet Width Below Channel	l_c	2	m
Latent Heat of Fusion	L	3.34×10^5	$\mathrm{J\ kg}^{-1}$
Clapeyron Slope	c_t	7.5×10^{-8}	$\mathrm{K\ Pa}^{-1}$
Specific Heat Capacity of Water	c_w	4220	$\mathrm{J\ kg}^{-1}\ \mathrm{K}^{-1}$
First Channel Flow Exponent	α_c	5/4	
Second Channel Flow Exponent	β_c	3/2	
Channel Source Term	Q_m	*	$\mathrm{m}^3\ \mathrm{s}^{-1}$

*this parameter is only used in the model runs with moulins, described in Section 3.4

3.2 Datasets

This section describes the various datasets that are used to model the current state and future of hydrology in the Wilkes Subglacial Basin hydrology. Topography of the region is required to be able to calculate hydraulic potential due to bed elevation, $\phi_m = \rho_w g B$, and pressure due to overlying ice (overburden pressure), $p_i = \rho_i g H$. Basal parameters like velocity, u_b, and melt rate, m, are required to determine ice-bed interactions that directly shape the distributed drainage system. The only dataset we have describing the future is the Surface Mass Balance (SMB) for the year 2100, which provides another source of water to the subglacial hydrology system. Datasets for all these parameters are used in modelling the subglacial hydrology system with the GlaDS model.

The topography of the region includes the bed topography (Figure 3.1a) and ice thickness (Figure 3.1b), the sum of which yields the surface elevation. We take these data from a 2019 version of BedMachine Antarctica, which describes topography for the entire Antarctic continent at a 500m resolution (Morlighem et al., 2020). This dataset was produced starting from empirically-derived ice thickness and surface velocity. Then, either mass conservation (MC) or streamline diffusion methods were used in various regions to compute the topography for the majority of Antarctica. This allows us to obtain topography for the entirety of the Wilkes Subglacial Basin from a single, consistent product.

Basal velocity (Figure 3.2a) and melt rates (Figure 3.2b) were derived from ice sheet modelling using the Ice-sheet and Sea-level System Model (ISSM) (Seroussi et al., 2020). Basal velocity is important for calculations of cavity opening rates in GlaDS as well as accurately modelling ice streams. Information about basal water sources in the form of basal melt is important as it is present in all glacial systems. It is also currently the dominant source for subglacial hydrology systems in Antarctica. Basal factors play the largest role in Antarctic subglacial hydrology today because the Antarctic climate is cold enough to prevent melting on the surface all year long. However, if global temperatures continue to increase due to climate change, which disproportionately affects the poles, we could see surface melt playing a role in the subglacial hydrology of the future (Meredith et al., 2019).

The only datasets we have used that corresponds to the future are predictions of the surface melt rate in Antarctica by the year 2100. The rest of the datasets are taken from current geographic knowledge of the region, which are used either assuming there will be no significant change or in lieu of projections. The future SMB datasets come from climate modelling which predicts the surface runoff rates in Antarctica. The method used to model the climate is to couple both the atmosphere and ocean over the entire globe to be able to account for global climate effects. However, there is no single definitive projection of SMB, and the resulting dataset we use depends on a couple of factors.

The first factor is the climate model used. Different climate models have been created and

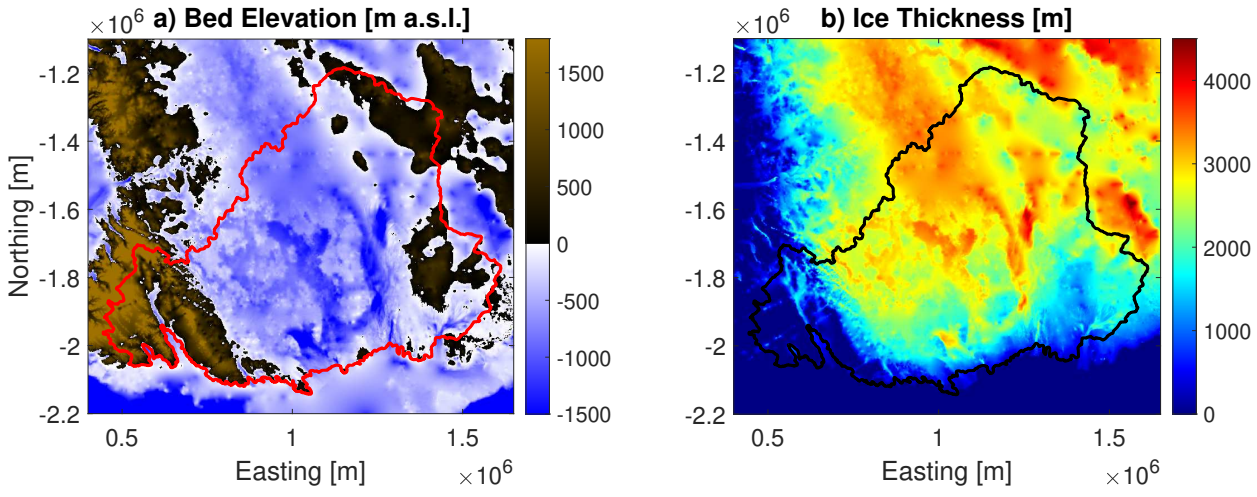

Figure 3.1: Topography in the Wilkes Subglacial Basin from BedMachine Antarctica (Morlighem et al., 2020). a) Bed elevation, B, in units of metres above sea level (m a.s.l.). Includes the model domain boundary outlined in black. The central region is below sea level while the eastern region (left) is a part of the Transantarctic Mountains. b) Ice thickness, H, which includes the model domain boundary outlined in black. Ice is thin along the grounding line located in the bottom of the domain, and gradually increases going up the domain towards the interior of Antarctica. The elevation of the surface is the sum of basal topography and ice thickness.

developed by different groups and institutions. These different climate models predict a wide range of future climate conditions, and thus produce different surface mass balance datasets for the year 2100. We consider a set of climate models from the Coupled Model Intercomparison Project 5 (CMPI5) that was analysed specifically for the Ice Sheet Model Intercomparison Project 6 (ISMIP6) by Barthel et al. (2020). The recommended climate models from CMIP5 for modelling in Antarctica had to perform well compared to all the other climate models in historical runs, as well as be representative of the average predicted future climate conditions. I then compared the recommended climate models with respect to one another in terms of the distribution and total volume of predicted runoff specifically for the Wilkes Subglacial Basin region. This led to the choice of the CCSM4 climate model.

The second factor that changes the surface runoff predictions are projections of the concentration of greenhouse gases in the atmosphere. For climate modelling, the Intergovernmental Panel on Climate Change (IPCC) developed a parameter that controls the greenhouse gas effect called the representative concentration pathway (RCP) scenario (Collins et al., 2013). Instead of talking directly about the concentration of greenhouse gases in the atmosphere over time, RCP scenarios instead describe an equivalent change in solar radiation being

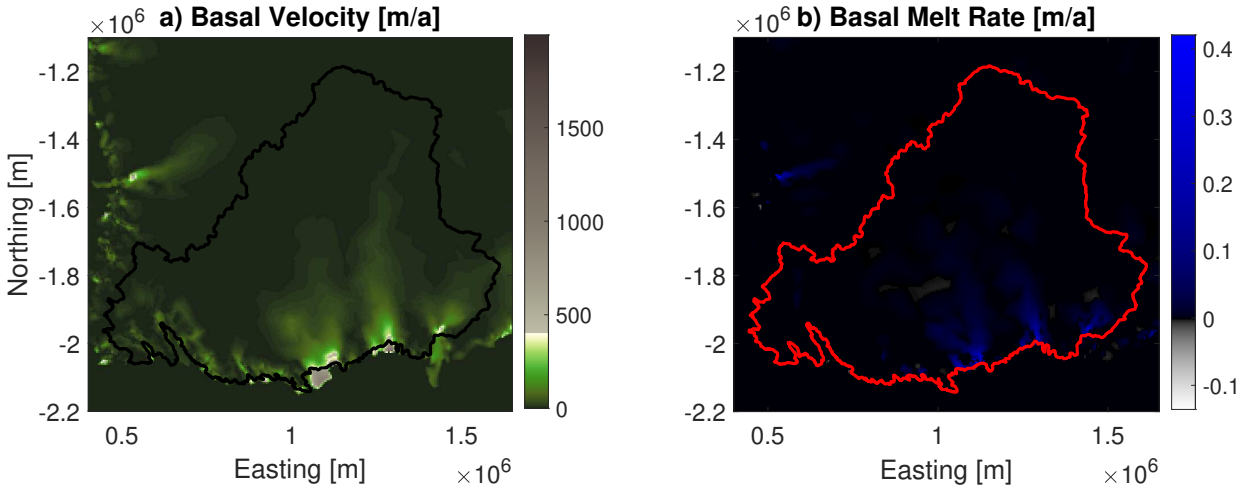

Figure 3.2: Basal parameters in the Wilkes Subglacial Basin, calculated in ISSM (Seroussi et al., 2020). a) Basal velocity magnitude, u_b, in units of metres per year or annum (m/a), with the model domain boundary outlined in black. The largest basal velocities are near the grounding line, and also correspond with the locations of the Mertz, Ninnis, and Cook Glaciers. b) Basal melt rate (component of m) with the model domain boundary outlined in red. Like basal velocity, the largest rates are near the grounding line and correspond with the locations of the Mertz, Ninnis, and Cook Glaciers.

captured by the atmosphere over time. The two main RCP scenarios considered in the datasets are RCP 2.6 and RCP 8.5, which correspond nominally to scenarios where the atmosphere absorbs that much net energy (in units W/m^2) by the year 2100. For modelling purposes, we ideally want to choose a SMB dataset that has both RCP scenarios available to be able to compare how the different climate scenarios affect runoff rates and subglacial hydrology. So, the factors we considered when choosing a SMB dataset for the Wilkes Subglacial Basin region are the climate model used and the RCP scenario it was trying to simulate. The runoff rates for the CCSM4 climate model under both RCP 2.6 and RCP 8.5 scenarios is plotted in Figure 3.3. Most of the differences between both RCP scenarios are located near the grounding line at the bottom of the domain, with the RCP 8.5 scenario having larger runoff magnitudes (noting the difference in colour map scales). This makes sense because again, the higher RCP scenario corresponds to a larger rate of solar energy absorption by the atmosphere in the year 2100, so a warmer climate which would increase melt rates.

To use the datasets that describe Antarctica and the Wilkes Subglacial Basin in the present and future, they need to be modified for input into the GlaDS model. As the GlaDS model is discretized by a triangular mesh, the next step is to create a mesh which the datasets are interpolated onto.

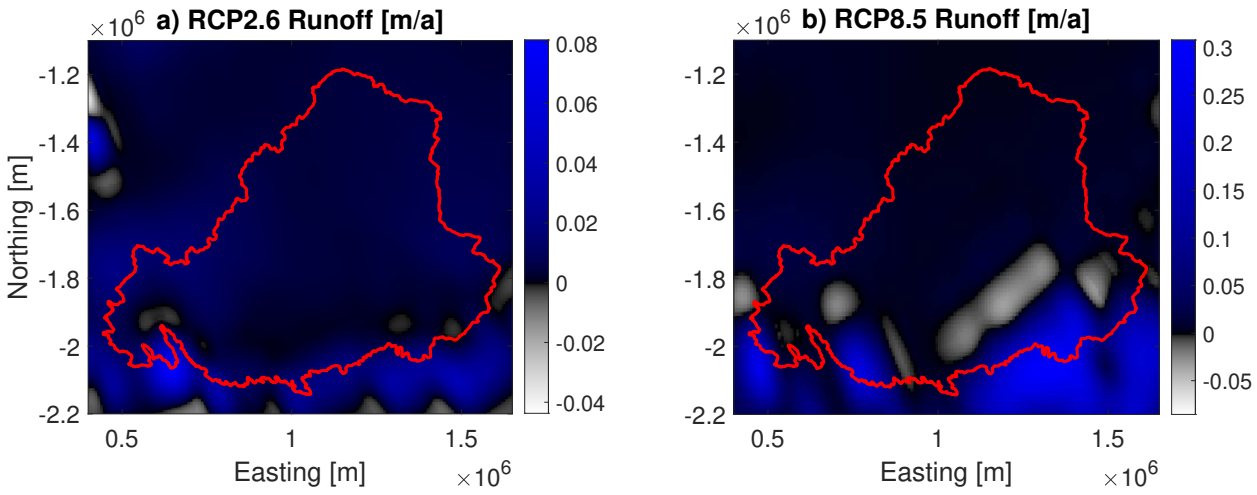

Figure 3.3: CCSM4 climate model surface runoff in the Wilkes Subglacial Basin. a) RCP 2.6 runoff rates with the model domain boundary outlined in red. b) RCP 8.5 runoff rates with the model domain boundary outlined in red.

3.3 Mesh

Although the region of interest aligns closely with the Australian Antarctic Territory districts of Oates Land and George V Land, we cannot use political boundaries. In order to model, and solve the equations with spatial derivatives, we need to set mathematical boundary conditions. The GlaDS model can implement mixed boundary conditions where both Dirichlet and Neumann type boundary conditions can be defined on distinct geographical features that dictates water flow. Along the grounding line we can apply a Dirichlet boundary condition by setting the hydraulic potential to be a constant, equivalent to the overburden pressure of ice that is now floating on the ocean. This works since we keep ice thickness to be a constant in space and time, and once we pass the grounding line and ice starts to float, there is no subglacial water pressure any more, replaced by buoyancy. Then, the rest of the boundary satisfies a Neumann boundary condition where we set the change in hydraulic potential to be equivalent to specifying no water flux across the boundary, by Equation 3.6. Geographically speaking, a boundary across which no water flows can be found at a drainage divide, the dividing line between two adjacent drainage basins. Therefore, our domain boundaries consist of the grounding line where it borders ice shelves, and subglacial drainage divides on land. This is how we can define the corresponding Dirichlet and Neumann boundary conditions.

To find subglacial drainage divides, I estimated the general direction of water flow at every point underneath the ice sheet. Estimating this requires assuming that the water pressure is at the ice overburden pressure and then calculating the subglacial hydraulic potential.

The hydraulic potential can then be used to find flow direction using the fact that water will flow from high pressure to low pressure. This will let us find the accumulation of subglacial water along specific flow routes, and break up our region into drainage basins, within which all water flows towards the same stretch of the grounding line, shown in Figure 3.4. We can then successively merge drainage basins until we cover as much of the grounding line as is inside our region of interest.

Once we get a complete boundary to satisfy the two boundary conditions, we can partition the domain into triangles. The triangles are irregular to avoid any systematic bias in subglacial channel formation, as the channel network develops along the mesh edges. The triangular mesh is also refined in regions where basal velocity is greater than 30 m/a. This is because we expect areas of high basal velocity to correspond with areas of high water pressure and hydrological activity. This also generally corresponds to steep troughs in the basal topography.

The final refined mesh (Figure 3.5) has a total of 40,058 elements or triangles, 20,463 nodes, and 60,520 edges, covering a total area of 6.13×10^{11} m^2. The average area of elements (summing all elements and dividing by the total number of elements) is 1.5309×10^{7} m^2, with the distribution being bimodal due to a peak around the normal element area of 1.625×10^{7} m^2, and another at the refined element area of 6.75×10^{6} m^2. The average edge length (summing each edge and dividing by the number of edges) in the mesh is around 6 km, with a peak in frequency at 5.5 km and 3.7 km, again corresponding to the normal and refined regions of the mesh. The average edge length along the grounding line section of the boundary, where it is generally more refined, is 4.2 km. There are a few outliers that have edge lengths less than a kilometre, with the minimum being 0.7 km.

Now that we have the mesh and node positions, we can determine the values of the input variables at each nodal position. A simple bilinear interpolation is used for each of the datasets discussed in the previous section: basal and surface topography, basal velocity and melt, and future SMB runoff.

3.4 Moulin Prediction

It is expected that as the climate continues to change and Antarctic air temperatures continue to rise, surface runoff will become a new hydrological source in Antarctica. This will pave the way for moulins to become common place as they already are in valley glaciers and the Greenland Ice Sheet today. The subglacial hydrology system will then be impacted by large volumes of water accumulated in supraglacial streams and reservoirs being redirected from the surface - through a moulin - to the bed. To more accurately model the subglacial hydrology of the future, we have developed a simple method to approximate number and location of moulins.

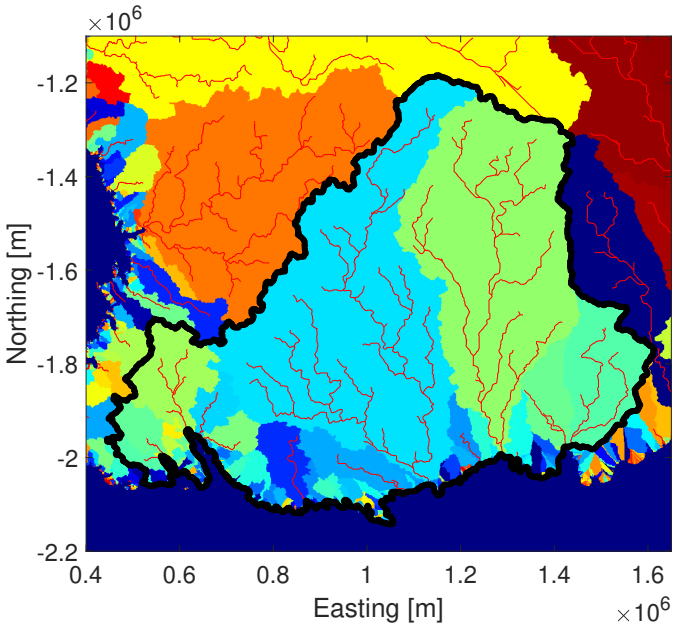

Figure 3.4: Map of the drainage basins of the Wilkes Subglacial Basin region. The region included in the model domain (outlined in black) is based on the collection of basins that drain to the section of the grounding line of interest. The paths with significant flow accumulation are plotted in red.

The method we have developed to find moulins takes into account a well understood method of moulin formation, which is the process of hydrofracturing (Das et al., 2008, Clason et al., 2015). Hydrofracturing occurs when an existing crevasse or fracture in the surface of a glacier is filled with water that exacerbates the crack. This can lead to a crevasse reaching all the way to the base of the glacier, where the water is then taken up by the subglacial hydrology system (van der Veen, 1998). Continued water flow into the crevasse forms a moulin which then acts as a near-vertical conduit for water from the surface to the bed. Crevasses naturally form on glaciers due to uneven flow of different sections of ice due to spatially varying bed topography (Benn & Evans, 2013). Common places this happens is along the margins of ice streams - lengths of ice that flow faster towards a glacier terminus than neighbouring sections - or as ice speeds up nearing a terminus, causing it to stretch away from ice further upstream. As long as there is differential motion within a glacier that creates an internal stretching or tensile force strong enough to overcome the fracture toughness of the ice itself, crevasses can form (van der Veen, 1998). Once a surface fracture exists, hydrofracturing can occur when the crevasses are inundated with water, for example when they are fed by a supraglacial stream of meltwater. This addition of water provides an additional force inside the crevasse that pushes outwards on the crack due to pressure generated by the weight of water above. If the initial crack is large enough and is filled with enough water, this process can drive the crevasse deeper and deeper in a positive feedback loop as the crevasse grows and more water is provided, until the base of the glacier is reached (van der Veen, 2007).

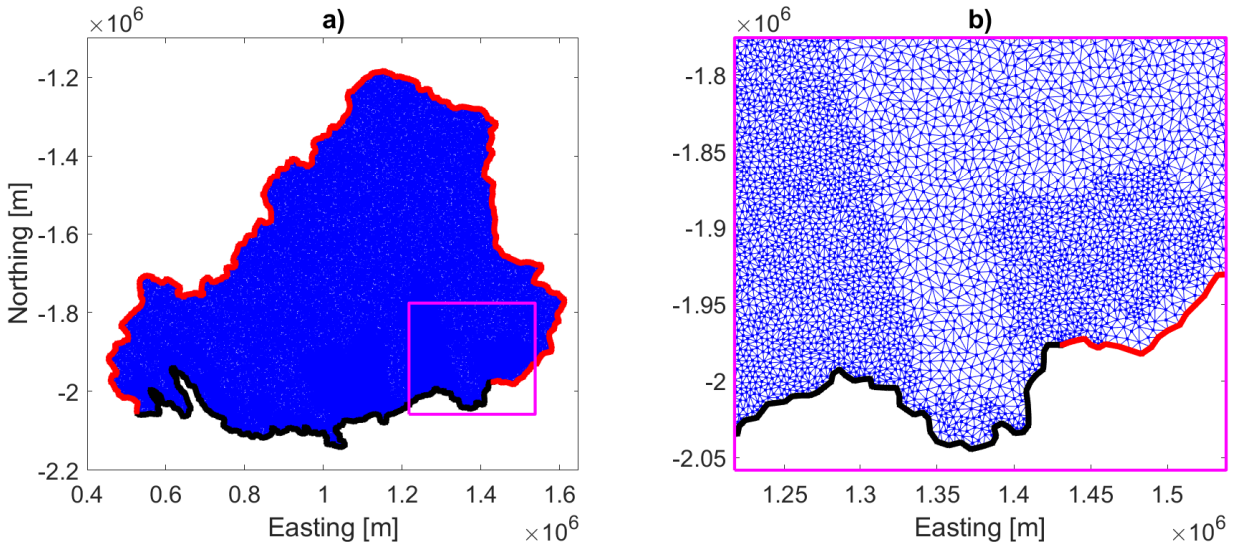

Figure 3.5: Wilkes Subglacial Basin irregular, triangular mesh created from the outline around drainage basins. a) Complete mesh with zoom-in region boxed in magenta. The boundary is split up into drainage divides that are plotted in red and the grounding line that is plotted in black. b) Zoomed-in region that shows an example of mesh refinement where there are faster basal velocities.

To account for the process of hydrofracture, our method takes into consideration variables for both initial crevasse formation and sufficient surface water reaching that crevasse. Then, we set thresholds for each variable and find all points in the domain that exceed both thresholds. These points are likely locations for hydrofracturing to occur. For initial crevasse formation, we set a threshold for longitudinal strain (tension) of the glacier. For sufficient water reaching a crevasse, we set a threshold for surface water accumulation. Strain rate can be calculated using surface velocities, and then the locations that exceed a fixed threshold can be found and set to be regions where large crevasses will likely form and be our possible locations for moulins. However, the same process can not be done for surface water accumulation, because the existence of a moulin cuts off the flow of water as it is rerouted to the base of the glacier. In other words, we are using accumulation to determine moulin locations, but the calculation of accumulation is also dependent on the position of moulins. So, it is not enough to just to do one calculation of surface water accumulation to determine a region that surpasses an accumulation threshold. The way to work around this dependency of water accumulation to moulin location is to use the fact that water accumulation at any one point is independent of accumulation at any other point downstream. This relationship between accumulation and moulin position informed us about how to build an algorithm to be able to determine locations of likely hydrofracturing and therefore moulins.

The process by which we determine moulin locations uses surface topography, velocity,

and runoff. Starting from the surface topography of the region and filling any holes or depressions, we can calculate the gravitational potential at every point in the domain. This is a simplification as it rules out accumulation into supraglacial features like firn aquifers or lakes, which in particular are known to promote hydrofracture underneath them. However, this would require additional modelling of filling and draining lakes, and calculations of the fracture point between the interaction of a sufficiently filled lake and an underlying crevasse. So, after filling depressions and sinks, we can determine the routing of water along the surface as simply the direction from every point to its neighbour with the lowest potential. Then, knowing the routing of water along the surface, we can start considering accumulation of surface water as the volumetric sum of all water generated upstream from any given point in the domain. We can then start to find moulin locations using accumulation and strain:

1. Starting at the highest potential in the domain going down, the first point that surpasses both accumulation and tension thresholds becomes a moulin.
2. Recalculate the surface accumulation using the fact that the new moulin reroutes all water accumulated up to it away from the surface.
3. Repeat steps 1-2 until there are no other points in the domain that pass both thresholds.

Moulin input rates are then calculated as the seasonal accumulation values at their respective locations. These values will eventually correspond to the external source input at each node, Q_m, which is included in the balance of the channel discharge connecting all adjacent channels (Eq. (3.19)). The difference between these moulin input rates and Q_m is that we apply a seasonality factor such that over the course of a modelled year, surface input only reaches the bed during a specified melt season. This is further discussed in the following section, which describes the process of running models in GlaDS.

3.5 Model Runs

I perform initial GlaDS model runs with basal meltwater as the only hydrological input to try and reach steady state. Typical steady state simulations run for 20,000 simulated days ($\sim$54 years), after which we compare the change in water thickness, h, between the two final time steps to determine if a steady state has been reached in the distributed drainage system. The steady state run is important to be able to find flow paths and channel locations that naturally develop a subglacial hydrological network according to the input topography and mesh. Steady state runs also help smooth out the process of modelling by removing transient behaviour due to introducing water into our system and to make sure that no major mistakes were made in inputting data and parameters. After a steady state has been reached, we can use the end state as the start for various runs with differing parameters.

Model Run	Climate Scenario	Moulins (Strain Threshold)	Acronym
Steady State (SS)	None	None	SS
Current	None	None	Current
Surface Straight to Bed (S2B)	RCP 2.6	None	S2B2.6
	RCP 8.5	None	S2B8.5
Surface through Moulins	RCP 2.6	Fewer (0.05)	FM2.6
	RCP 8.5	Fewer (0.05)	FM8.5
	RCP 2.6	More (0.01)	MM2.6
	RCP 8.5	More (0.01)	MM8.5

Table 3.3: List of different surface water input scenarios tested. Climate scenarios are described in Section 3.2, and moulin strain thresholds are described in Section 3.4.

We test a wide range of scenarios to determine the impact of a future SMB runoff source in the Wilkes Subglacial Basin, which is summarized in Table 3.3. The first case is without any surface water source, keeping the water input limited only to the spatially variable basal melt rate. This scenario corresponds to the current state of water sources in Antarctic subglacial hydrological systems, or also the case where there is no surface runoff in the future. The next case is where there is a surface runoff contribution to the hydrological system that is sent straight from the surface to the bed (S2B). This case is run for each of the two RCP scenarios from the chosen CCSM4 dataset of runoff (as described in Section 3.2). This is the simplest way to introduce surface meltwater to the bed as moulin formation and position do not have to be taken into account. However, this is really only applicable if there is widespread access for surface water to drain to the bed like in a heavy crevasse field. Otherwise normally, surface water will first drain through the supraglacial hydrology system due to the impermeability of ice. This is considered in the final case which lets a surface runoff contribution pass through a simple supraglacial hydrology system before being sent down moulins. The number of moulins and locations are predetermined using the process explained in the previous section. Again, each RCP scenario is run in this case, corresponding to different levels of surface runoff by the year 2100. The big modelling difference between directly sending surface water to the bed and sending surface water only down moulins is that the latter creates much more concentrated and localized sources to the bed. Also in the S2B case, the domain for surface melt input is identical to the domain of the subglacial hydrological system, while in the moulin case, the domain for surface melt input can be more realistically set to that of supraglacial drainage basins. In effect, this allows surface meltwater further inland than the (basal) mesh domain to be incorporated into the model as it flows over the basal drainage divides on the surface, and some surface meltwater near the grounding line to be excluded as it flows over the grounding line from the surface onto ice shelves. These three cases that change how water is incorporated into the GlaDS runs gives us the ability to compare what affects the different water sources have.

Since surface melt depends heavily on the seasons, annual rates will not be distributed uniformly throughout a year. To be able to account for seasonality in SMB inputs into GlaDS, we have concentrated the annual SMB runoff rates into three months defined as

the summer melt season. Keeping the total annual volume of surface meltwater the same, the inputs into GlaDS are scaled into a single sinusoidal period starting and ending at zero at the beginning and end of the melt season, and peaking during the middle of the melt season (Figure 3.6). These scaled annual moulin inputs are then the values of the external source applied to their respective nodes, Q_m, in the coupling between adjacent channels. There is no surface melt water input into the subglacial hydrological system outside the melt season, and the same distribution is repeated twice for two year transient runs.

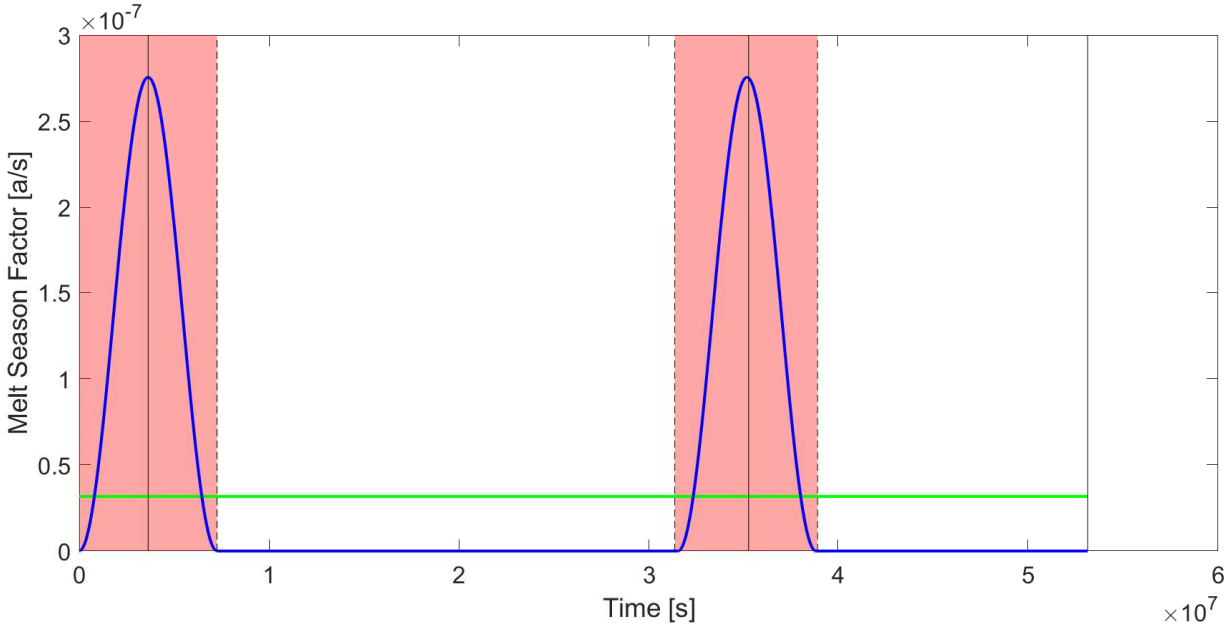

Figure 3.6: The melt season factor is the scaling factor on annual water inputs in order to simulate melt seasons when converting units from years to seconds. A temporally constant melt season factor used for basal melt water is plotted in green. An annual three month melt season factor used for surface runoff is plotted in blue. Solid, black vertical lines show the melt season peaks and the end of the model run. Dashed lines denote the beginning and end of the melt seasons which are also highlighted with a red background.

Chapter 4

Results

This chapter will cover the results of the project starting in Section 4.1 with the moulin locations that were calculated for the Wilkes Subglacial Basin using the algorithm discussed in Section 3.4. This is followed by Section 4.2 looking at the subglacial hydrology outputs from GlaDS model runs of the various scenarios described in Section 3.5.

4.1 Moulin Prediction

Moulin locations were calculated using current elevation and velocities, and future runoff predictions from the surface of the Wilkes Subglacial Basin region as discussed in Section 3.4. Thresholds for strain rate and water accumulation were set as a simple measure for moulin formation by hydrofracture. The value chosen for the accumulation threshold is 5 m^3/s, taken as a typical discharge rate of a moulin. By using this value, the assumption being made is that moulins with a smaller discharge rate do not provide enough water for hydrofracturing to occur. The value for the strain threshold is more difficult to determine and justify. The minimum strain required to create a fracture in an ice sheet is not a well constrained quantity and varies widely depending on local conditions of the ice for an empirical value (Vaughan 1993), or mathematical model and complexity for a theoretical value (Lai et al., 2020, van der Veen, 1998). To get around this, we tested many different strain thresholds, including no strain threshold at all. Different values were then chosen to try and capture a wide, realistic range in number and density of moulins for the region. Specifically, the values 0.05 and 0.01 were chosen to represent scenarios with fewer and more predicted moulins respectively. A higher strain threshold means a smaller section of the domain is deemed capable of producing a fracture. These two strain thresholds, in combination with the two RCP scenarios, which change the magnitude and spatial distribution of runoff, makes a total of four different sets of predicted moulins. From now on these moulin sets and scenarios are referred to as Fewer Moulins RCP 2.6 (FM2.6), Fewer Moulins RCP 8.5 (FM8.5), More Moulins RCP 2.6 (MM2.6), and More Moulins RCP 8.5 (MM8.5).

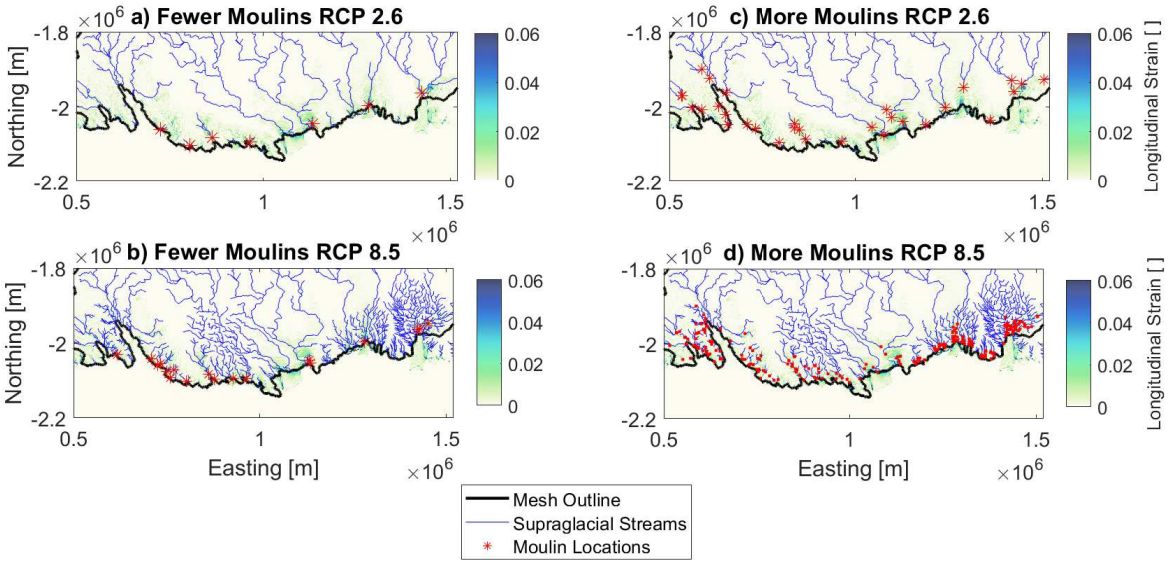

Figure 4.1: The positions of the calculated moulins for each moulin scenario: a) FM2.6; b) FM8.5; c) MM2.6; and d) MM8.5. They are plotted on a map of the longitudinal strain or tension, with the mesh outline in black and significant supraglacial flow routing in blue. The size and type of the red point markers for the moulin locations change between each plot only to improve visibility depending on the density of moulins.

These moulins are plotted in Figure 4.1, on top of a map of strain rates, which is the same in each of the four scenarios. A summary of the sets can be found in Table 4.1 showing number of moulins and the total accumulation rate that reaches them for each scenario. The number of moulins predicted by each scenario increases with both the higher RCP scenario and lower strain threshold. The FM2.6 scenario has 7 moulins while the FM8.5 scenario has 19 moulins. The MM2.6 scenario predicts 31 moulins compared to 214 moulins for the MM8.5 scenario. The difference in moulin locations based on the different strain threshold is that the MM scenarios have a larger subsection of the domain where moulins are allowed to form compared to the FM scenarios, as long as the accumulation threshold is reached. The difference in moulin locations based on the different RCP scenarios is then that within the same subsections, a higher RCP scenario with a higher runoff rate causes supraglacial streams to recharge faster, surpassing the accumulation threshold more often. This results in a greater density of moulins within the same region. Comparing the accumulation rates, the FM2.6 scenario moulins captures the lowest rate of surface runoff, while the MM8.5 scenario captures the highest rate. Then between the middle two scenarios, the FM8.5 scenario captures a slightly higher rate than the MM2.6 scenario, even though the MM2.6 scenario has more moulins.

Moulin Scenario	RCP Scenario	Accumulation Threshold [m^3/s]	Strain Threshold [ ]	Number of Moulins	Total Accumulation [m^3/s]	Moulin Average [m^3/s]
FM	2.6	5	0.05	7	486.75	69.54
FM	8.5	5	0.05	19	2,202.00	115.89
MM	2.6	5	0.01	31	1,797.80	57.99
MM	8.5	5	0.01	214	7,513.50	35.11

Table 4.1: Description of the sets of moulins for each of the four moulin scenarios.

4.2 Subglacial Hydrology

This section will now look at the subglacial hydrology outputs from GlaDS model runs as described in Section 3.5. Described first is the Steady State (SS) run to create a steady starting point for the rest of the model runs performed. The next model run discussed is the Current run, which uses the same parameters as the SS, whose outputs will be used as the baseline to compare all the future runs that include predicted surface water input by the year 2100 from the CCSM4 climate model. The rest of the section is broken down by GlaDS model output where water pressure, water thickness, and channel discharge will be considered one at a time.

4.2.1 Steady State and Current Run

To ensure model outputs aren't affected by transient startup behaviour, we first run until we reach a SS. The only water input for the SS run is from the temporally constant subglacial melt rate, which is added into the distributed drainage system. SS is reached when there is little difference in the water thickness, h, between time steps, and the distributed drainage system is balancing the constant subglacial melt being produced with the water flowing over the grounding line and leaving the system.

As the water thickness in the distributed drainage system is defined for every node in the mesh, we can do a spatial analysis of the water thickness difference, Δh, as shown in Figure 4.2. The colour of each node (plotted as individual points) corresponds to the final difference in water thickness at that node after the 20,000 days modelled in the SS run. There are only two points in the whole domain that have water thickness differences greater than 1×10^{-4} m, also highlighted with red circles. They are both in the Cook Ice Shelf subglacial catchment near the grounding line. As will be shown in Section 4.2.4, they are also located where there are subglacial channels, although there are also other nodes that have channels along with smaller final water thickness differences. There is a large central region of the domain that has final water thickness differences between 1×10^{-6} m and 1×10^{-4} m, marked in yellow. They are located in the catchments of Cook Ice Shelf and Ninnis Glacier. Most of the nodes near the grounding line have water thickness differences less than 1×10^{-8} m, in green, with the rest of the domain being between 1×10^{-8} m and

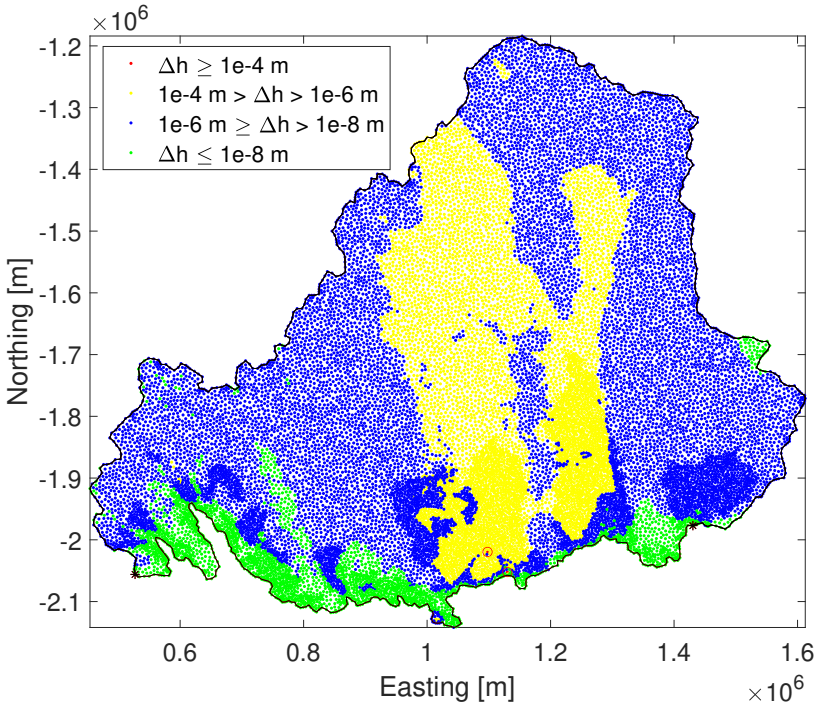

Figure 4.2: Water thickness difference (Δh) between the final two timesteps of the SS run in units of metres. All nodes are plotted with colours corresponding to the magnitude of the difference. The two nodes with difference greater than 1×10^{-4} are also circled for visibility. The domain boundary is plotted in black, with the grounding line section marked as between the black stars.

1×10^{-6} m in blue.

We can also plot the water thickness over time at each node, shown in Figure 4.3, using the same colour scheme based on the difference in water thickness between the last two timesteps. This shows an initial increase in water thickness for a lot of nodes as the subglacial hydrology system initializes. At the end of the run most nodes have reached a plateau with at most a slight, constant decrease in water thickness. This is also true of the two red nodes (with final water thickness greater than 1×10^{-4} m), which gives us confidence that we have reached a SS.

From the SS, we first run a control, base run where no additional water source is added, so all parameters are identical to that of the SS run. This is called the Current run because the only water input into the subglacial hydrology system is from basal melt, which is currently the only subglacial hydrology source for the majority of Antarctica. This Current run is set to go for one year and nine months, fully encompassing two melt seasons, just like all subsequent runs. As expected, outputs from this base run are constant and steady throughout this extra time, and are identical to the outputs from the steady state run.

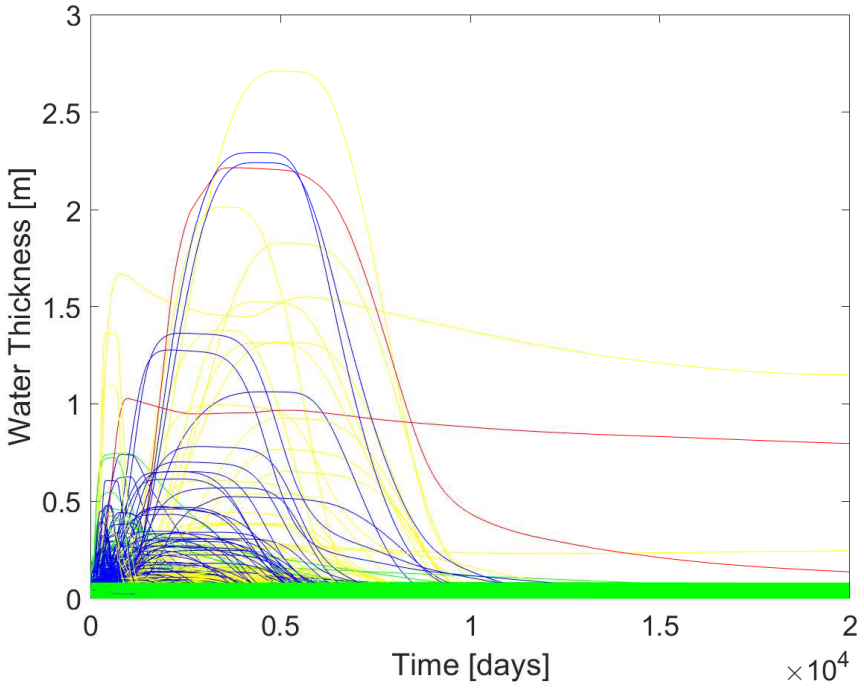

Figure 4.3: Time series of the water thickness output at each node in the SS run. Colours correspond to the difference between the final two timesteps as outlined in Figure 4.2.

4.2.2 Water Pressure

The first model output we will look at is the subglacial water pressure, p_w, which is plotted as a percentage of the overburden pressure of the overlying ice sheet. In other words, water pressure equal to overburden pressure counts as 100%, and corresponds to the point where ice uplift starts.

The water pressure from the Current run, which is used as the baseline from which all other model runs are compared, is shown in Figure 4.4. The plot is of the entire domain at the final timestep, but since the Current run is an extension of the SS, plotting any timestep would yield similar results. Starting by looking at the grounding line, there are high water pressures (>80%) corresponding to the regions of the Cook, Ninnis, and Mertz outlet glaciers. The Matusevich and Rennick glaciers are also visible at the grounding line as distinct regions of higher water pressure in contrast to either side along the grounding line. Moving away from the grounding line, Matusevich and Rennick glaciers also have a strip of distinctly higher water pressures from the grounding line up into the interior of the domain. High water pressures (>80%) are also present throughout most of the Cook and Ninnis subglacial catchments, even near the top of the domain. This is similar to the region of final water thicknesses between 1×10^6 and 1×10^4 m (coloured yellow in Figure 4.2). This likely shows the impact that topography has on the subglacial hydrology system as the region corresponds with basal topography below sea level found in the middle of the

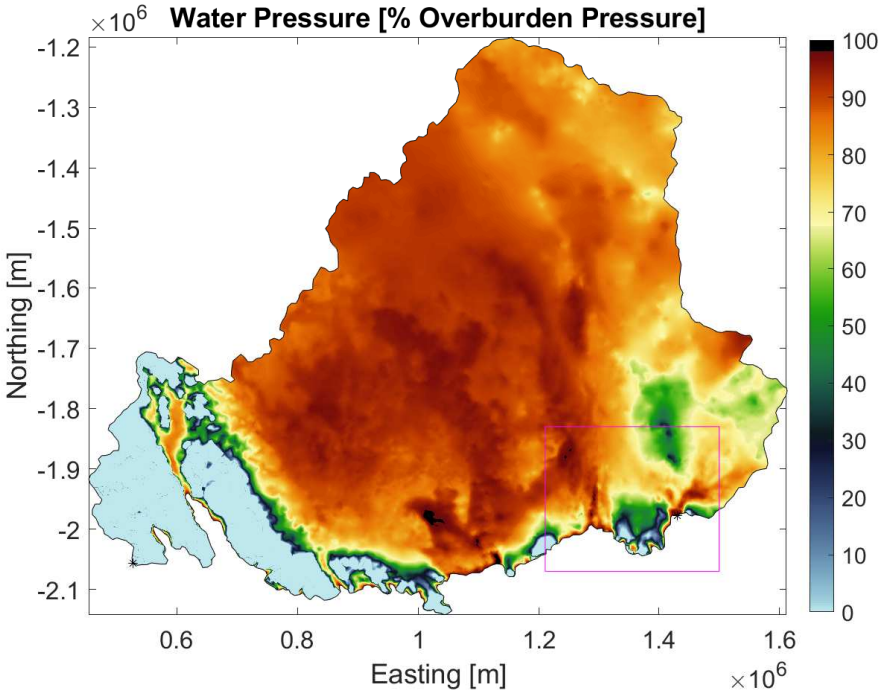

Figure 4.4: Water pressure from the Current run, where there is no surface water input into the subglacial hydrology system. Boxed in magenta is the region around Ninnis and Mertz glaciers used for Figures 4.7, 4.8, and 4.9.

domain (Figure 3.1).

Topography is also likely why most of the region around Ninnis and Rennick have unphysical, negative water pressures (cutoff at 0% in Figure 4.4). Since this region is a part of the Transantarctic Mountains, a lot of the region has bed elevations over 1 km above sea level along with no ice (so zero ice thickness, Figure 3.1). Since the GlaDS model simulates subglacial hydrology, without any ice there is no ice overburden pressure to calculate drainage from the interplay between overburden and water pressures. This is why the model outputs in this region should be interpreted with caution.

The six other model runs that we will be comparing to this Current run all have the future surface runoff as an additional source of water. As outlined in Section 3.5, they are the four moulin scenarios FM2.6, FM8.5, MM2.6, and MM8.5 including both RCP values for the Straight To Bed (S2B) scenario, from here on referred to as S2B2.6 and S2B8.5. Important to note again, unlike the SS and Current model runs, these future scenario model runs do not have temporally constant water inputs. For spatial plots that only show one timestep, the specific timestep plotted will be important to consider now. Figure 4.5 shows water pressure difference plots between the future scenarios and the baseline Current run at the peak of the second modelled melt season (out of two). The first thing to notice is that both S2B model runs (Figure 4.5a, b) have larger water pressure throughout the entire

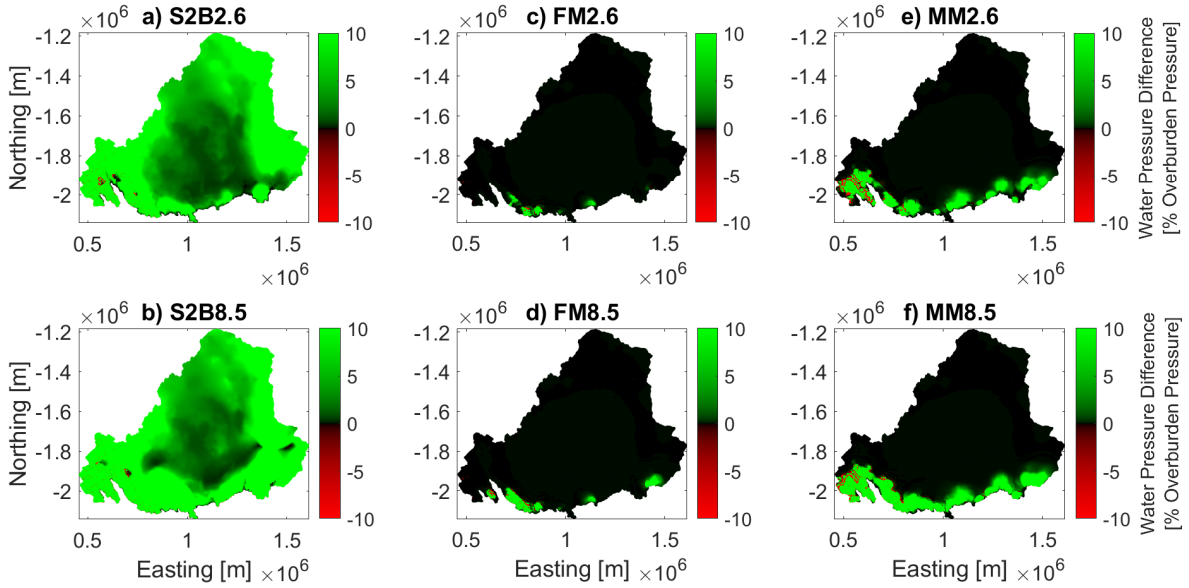

Figure 4.5: Plots of water pressure at the peak of the second melt season from the six future condition runs: a) S2B2.6; b) S2B8.5; c) FM2.6; d) FM8.5; e) MM2.6; and f) MM8.5. They are all compared to the Current run (Figure 4.4), which has been subtracted from them.

domain compared to the Current run. Outside of the central basin, this increase in water pressure is mostly greater than 10% overburden pressure. In the Transantarctic Mountain part of our domain we see the highest (and unphysical) water pressure differences reaching up to 1.6×10^{8}% and 2.0×10^{8}% overburden pressure (S2B2.6 and S2B8.5 respectively), which further highlights the difficulty in modelling those regions. We will consider more closely values of water pressure in Figure 5.3 which looks at averages of water pressure in restricted regions. The moulin runs also see larger water pressures, but only near the grounding line. Between the FM and MM runs (Figure 4.5c, d and e, f respectively), the MM outputs show a much more widespread coverage of water pressure increases greater than 10%, restricted to the grounding line. The FM outputs have the increases localized to the Cook and Matusevich glaciers, and Mertz glacier for FM8.5.

Figure 4.6 also shows difference plots of water pressure similar to Figure 4.5 but instead of at the peak of the second melt season it shows the final timestep near the end of the second year. Widespread increases in water pressures are still seen well after the end of the second melt season and the end of the future surface runoff inputs. There are noticeable pattern changes near the grounding line though, where in the S2B runs (Figure 4.6a, b) there is a thin region along the boundary that has dropped back to the baseline water pressure. In the moulin runs there is a different pattern where some spots that had an increase in water pressure during the melt season now experience a decrease in water pressure from baseline. This is observed at Cook glacier for all four moulin scenarios, at Mertz for all

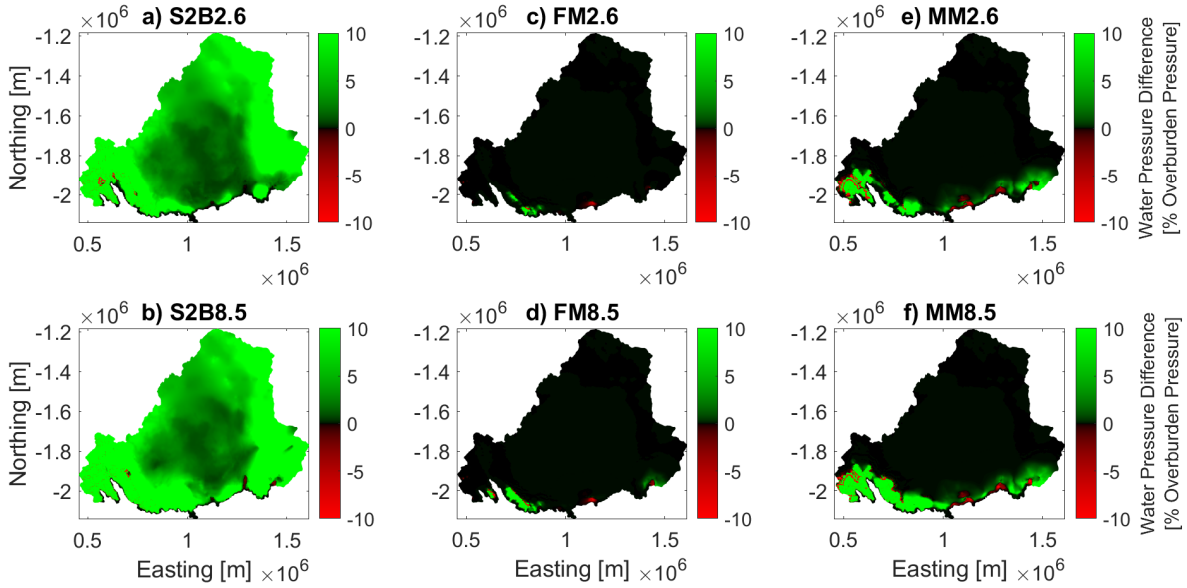

Figure 4.6: Plots of water pressure at the end of the second year (after the winter season) from the six future condition runs: a) S2B2.6; b) S2B8.5; c) FM2.6; d) FM8.5; e) MM2.6; and f) MM8.5. They are all compared to the Current run (Figure 4.4), which has been subtracted from them.

moulin scenarios except FM2.6, and also at Ninnis for both MM scenarios. This decrease in water pressure compared to the Current run signifies channelization, which draws in water from the surrounding distributed drainage system and lowers water pressures. Channel formation will be discussed further when looking at the model output of channel discharge in Section 4.2.4.

For the next difference plots of water pressure in Figure 4.7, we zoom into the Ninnis and Mertz glacier region (highlighted in Figure 4.4) and look at a time series of only the S2B8.5 scenario. The timesteps shown correspond to important points within the two melt seasons that are modelled from the peaks and ends of the melt season to the end of the year just before the start of the next melt season. A clear pattern emerges for water pressure at both Ninnis and Mertz, with the high water pressures as explained previously at the peak of the melt seasons. However, after the melt season when the extra surface water inputs decrease and remain zero, regions of negative water pressures are observed as channelization occurs. This region of negative water pressure at Ninnis has a straight and vertical profile whereas the negative region around Mertz stays around the grounding line.

Similar time series of Ninnis and Mertz glaciers are shown for the FM8.5 and MM2.6 water input scenarios in Figures 4.8 and 4.9 respectively. These two scenarios are interesting to compare to analyse the impact of changing to a higher RCP scenario and higher surface

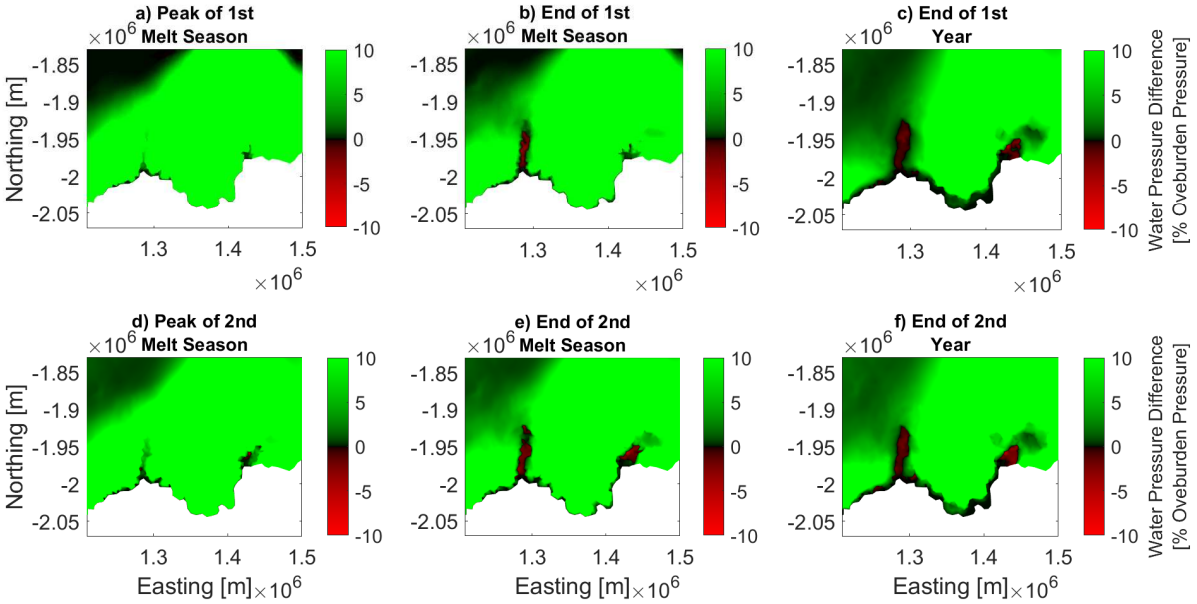

Figure 4.7: Plots of water pressure from the S2B8.5 model run focusing on the Ninnis and Mertz Glaciers over time: a) peak of, and b) end of the first melt season; c) end of the first year; d) peak of, and e) end of the second melt season; and f) end of the second year. The Current run (Figure 4.4), which has been subtracted from them.

runoff versus a lower strain threshold and more moulins instead. Both show the same pattern of a positive difference in water pressure changing to negative outside the melt season. In FM8.5 however, this is only seen in Mertz and in fact, there is no change from the baseline water pressure at Ninnis glacier. In MM8.5 this pattern is observed at both Ninnis and Mertz. This shows that Ninnis glacier is affected more by an increase in number of moulins and locations of water input rather than an increase in water input rates from the higher RCP scenario. Another interesting thing that we can see in the time series of Ninnis in the MM2.6 scenario is a wave in negative water pressure starting about 50 km away from the grounding line and moving towards it throughout the non-melt season (Figure 4.12b to c, and e to f).

4.2.3 Water Thickness

Next we can look at the water thickness, h, which corresponds to the volume of water in the distributed drainage system. The baseline water thickness from the Current run is plotted in Figure 4.10. The water thickness peaks at slightly over 1 m near the grounding line at Cook West glacier, however most of the domain has a water thickness of either 0 m or around 0.2 m.

The first set of water thickness difference plots in Figure 4.11 are from the peak of the

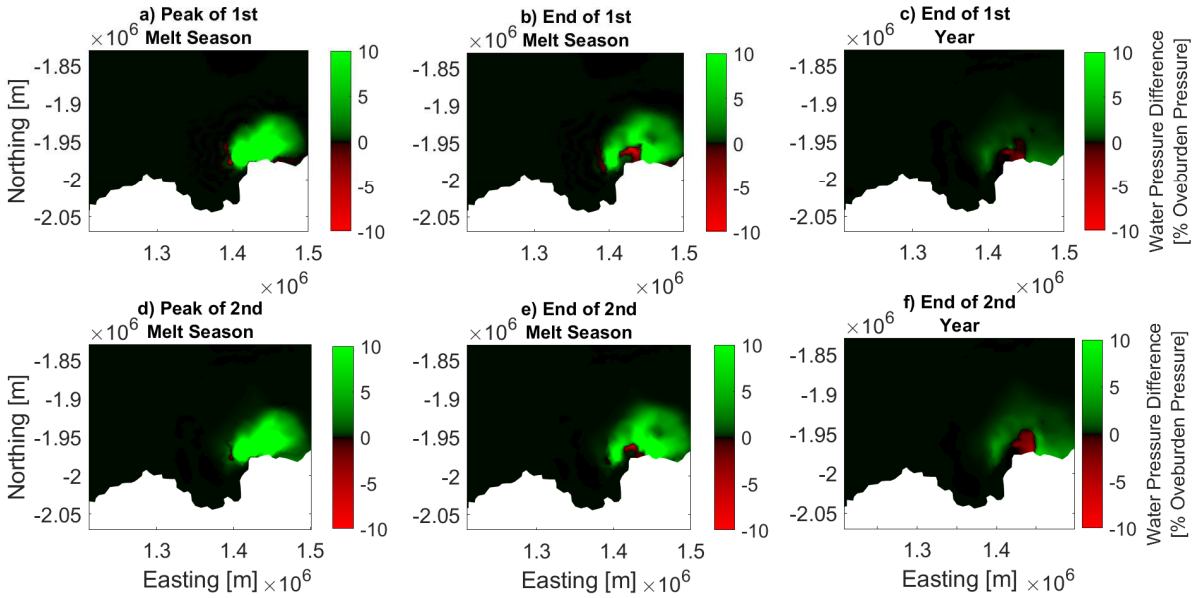

Figure 4.8: Plots of water pressure from the FM8.5 model run focusing on the Ninnis and Mertz Glaciers over time: a) peak of, and b) end of the first melt season; c) end of the first year; d) peak of, and e) end of the second melt season; and f) end of the second year. The Current run (Figure 4.4) has been subtracted from them.

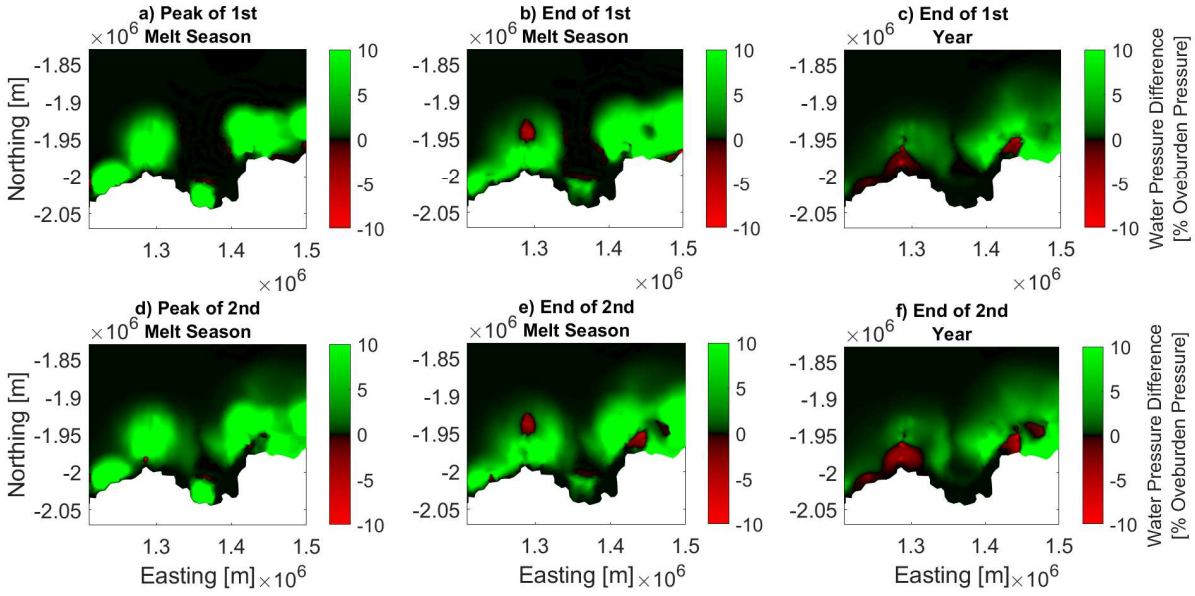

Figure 4.9: Plots of water pressure from the MM2.6 model run focusing on the Ninnis and Mertz Glaciers over time: a) peak of, and b) end of the first melt season; c) end of the first year; d) peak of, and e) end of the second melt season; and f) end of the second year. The Current run (Figure 4.4) has been subtracted from them.

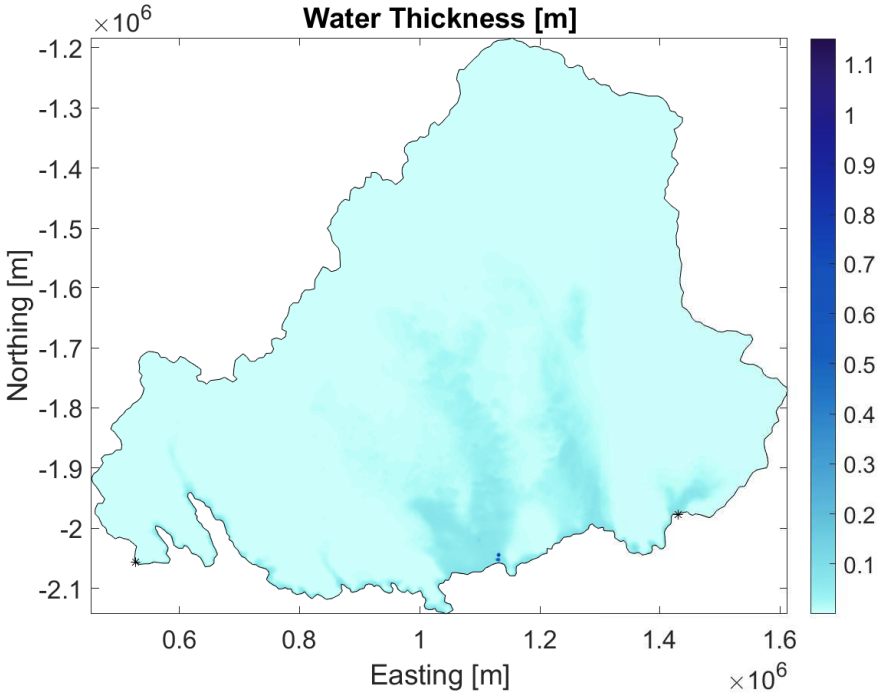

Figure 4.10: Water thickness from the Current run, where there is no surface water input into the subglacial hydrology system.

second melt season for the future runs. Like water pressure, the S2B runs show widespread increases throughout the entire domain compared to the Current run, whereas the moulin runs only show increases at specific regions along the grounding line. All RCP 8.5 scenarios show an increase in water thickness compared to their otherwise equivalent RCP 2.6 scenarios. Comparing the FM runs to the MM runs, the increases are more widespread with higher magnitudes in the MM runs. Similar to the water pressure, the Ninnis glacier region differs from the Current run only in the MM runs, and not the FM runs.

Figure 4.12 shows another water thickness plot, but this time at the end of the model run for the future scenarios. Similar to the changes in water pressure at the same timestep, water thickness does not change a lot from the peak of the second melt season, except for specific regions that show a negative instead of positive difference compared to the baseline. This is seen in most of the scenarios except S2B2.6 and FM2.6, in various combinations of the Cook, Ninnis and Mertz glacier regions.

4.2.4 Channel Discharge

The next model output we will look at is channel discharge, Q, which is a representation of the channelized drainage system. Figure 4.13 shows the channel discharge of the Current run, where only edges with a discharge greater than 1 m^3/s are considered channels and plotted. Most of the domain has no channelization except near the Cook, Ninnis, and

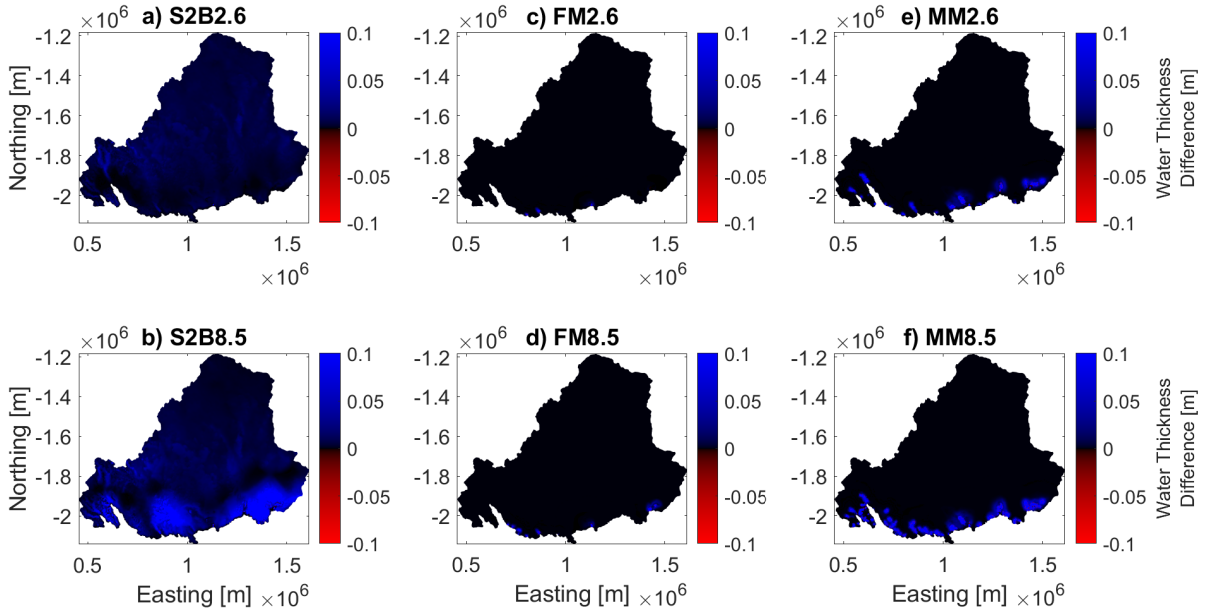

Figure 4.11: Plots of water thickness at the peak of the second melt season from the six future condition runs: a) S2B2.6; b) S2B8.5; c) FM2.6; d) FM8.5; e) MM2.6; and f) MM8.5. The Current run (Figure 4.10) has been subtracted from them.

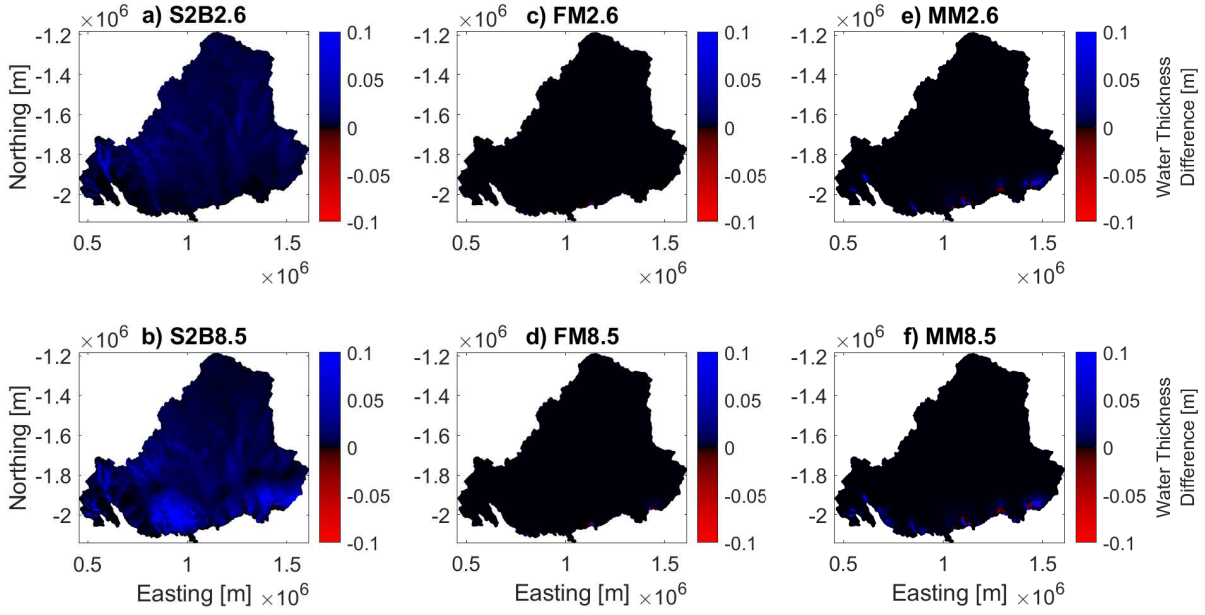

Figure 4.12: Plots of water thickness at the end of the second year from the six future condition runs: a) S2B2.6; b) S2B8.5; c) FM2.6; d) FM8.5; e) MM2.6; and f) MM8.5. The Current run (Figure 4.10) has been subtracted from them.

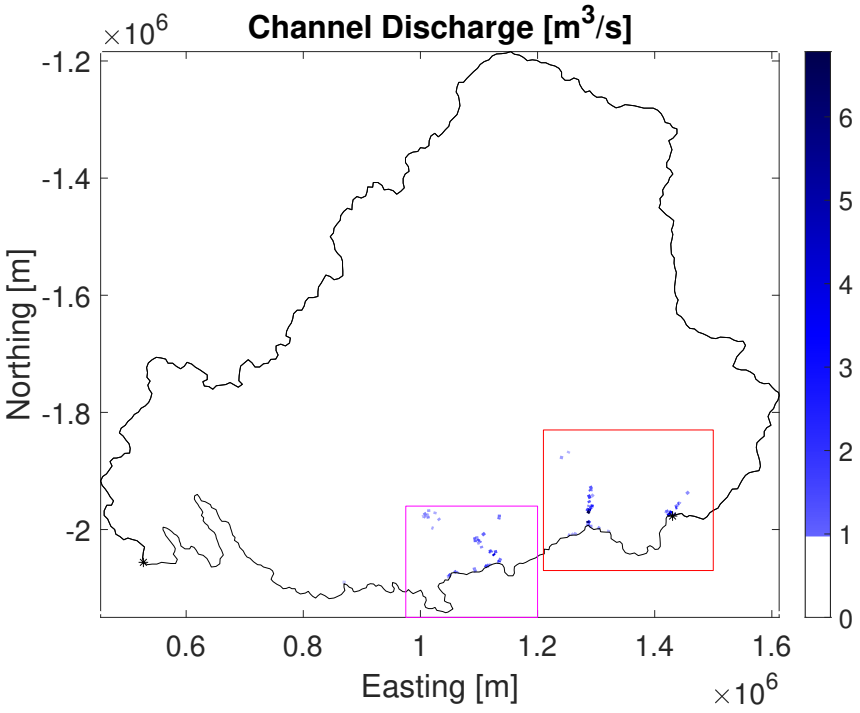

Figure 4.13: Channel discharge from the Current run, where there is no surface water input into the subglacial hydrology system. Only mesh edges with channel discharge greater than 1 m^3/s are plotted. Boxed in red is the region of the Ninnis and Mertz Glaciers used for Figures 4.15 and 4.16, and boxed in magenta is the Cook Ice Shelf region used for Figures 4.17 and 4.18.

Mertz glaciers. Two regions are highlighted and boxed for future plots looking specifically at the Cook region or the Ninnis and Mertz region.

Figure 4.14 shows the difference in channel discharge at the peak of the second melt season. Unlike water pressure and water thickness, the S2B runs only differ from the Current run near the grounding line and not throughout the upper domain as well. In fact, the S2B2.6 run shows very little difference spatially and none greater than 1.8 m^3/s. The S2B8.5 difference plot shows a clear increase at most glaciers including Mertz, Ninnis, Matusevich, Rennick, and Lillie, but not at Cook. This is in contrast with both FM runs where there isn't much difference except at Cook, where it also does not extend inland at all, remaining close to the grounding line. The MM runs do see increases at all the glaciers.

Still looking only at the peak of the second melt season, Figure 4.15 zooms into the Ninnis and Mertz regions as highlighted in Figure 4.13. For both FM runs (Figure 4.15c, d), the only difference from the Current run is Mertz glacier immediately inland from the grounding line. For both MM runs(Figure 4.15e, f), channel discharge increases are seen at both Mertz and Ninnis glaciers. While the Ninnis channels seem to clearly form as a straight line, the Mertz region channels appear in a much more dispersed area without as

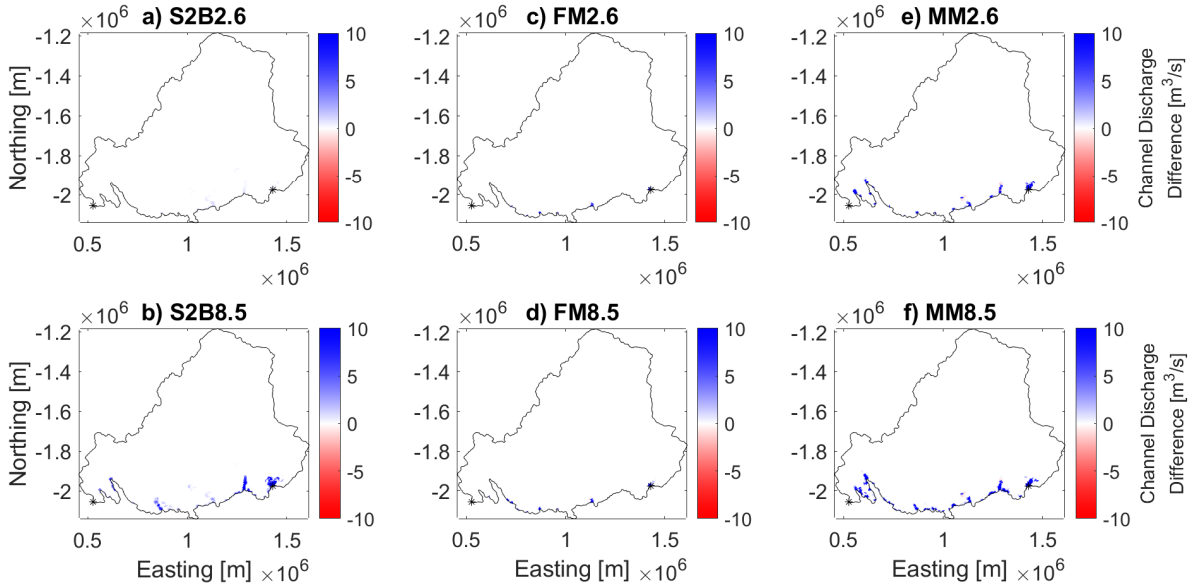

Figure 4.14: Plots of channel discharge at the peak of the second melt season from the six future condition runs: a) S2B2.6; b) S2B8.5; c) FM2.6; d) FM8.5; e) MM2.6; and f) MM8.5. The Current run (Figure 4.13), which has been subtracted from them.

clear a direction.

Next, Figure 4.16 looks at the same region but now at the end of the model runs, after around six months have passed since the end of the last melt season. While the channel discharge does not decrease a lot compared to the peak of the melt season, there are still some notable changes. The first one is that in the S2B8.5 and MM8.5 runs (Figure 4.16b, f), the increases in channel discharge along the grounding line beside Ninnis have mostly disappeared. This shows that without extra water input, channels in these regions can close back up. Also, for the S2B8.5 and both MM runs (Figure 4.16b, e, f), the straight channel section at Ninnis sees decreases mostly at the upper section of the channel farthest from the grounding line. This shows that while the Ninnis channel is still active after the melt season, it is becoming shorter. This effect isn't seen for the channels around Mertz glacier, suggesting that they behave differently from the channels around Ninnis and are not affected as much by the absence of surface water inputs.

The next Figures 4.17 and 4.18 show the Cook Ice Shelf region at the peak of the second melt season and at the end of the second year. For all S2B plots between these two timesteps, there is a change in channel discharge located along the grounding line and extending upstream from Cook West glacier, however the magnitude of the changes are small compared to those in the moulin runs. Also, looking at all the moulin runs, the change in RCP scenario has minimal impact on the channel discharge. Both FM runs

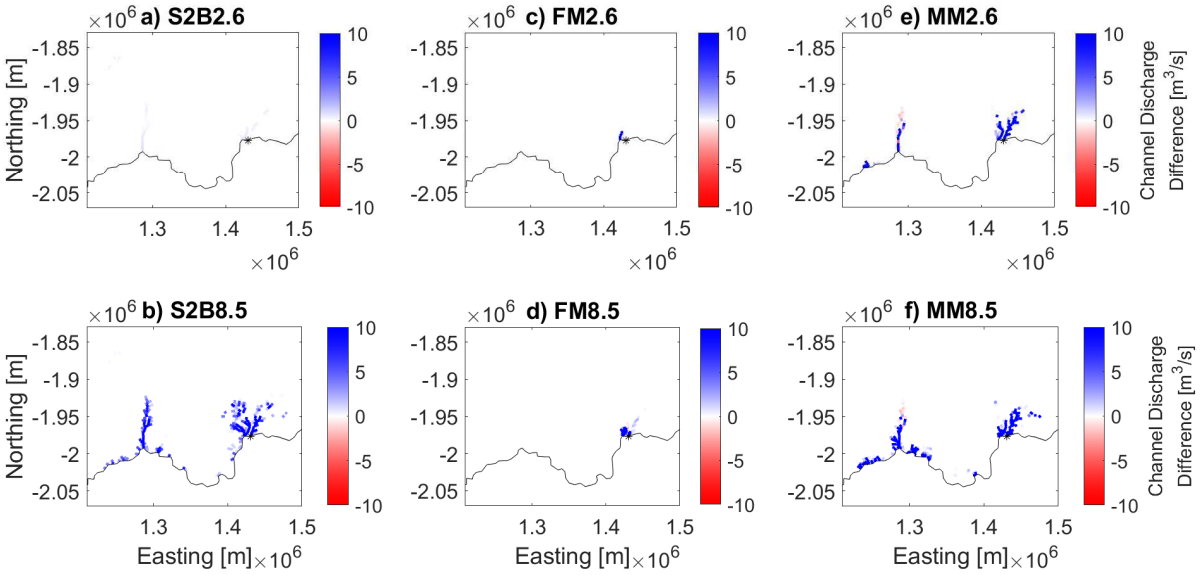

Figure 4.15: Plots of channel discharge at the peak of the second melt season focusing on the Ninnis and Mertz Glaciers from the six future condition runs: a) S2B2.6; b) S2B8.5; c) FM2.6; d) FM8.5; e) MM2.6; and f) MM8.5. The Current run (Figure 4.13) has been subtracted from them.

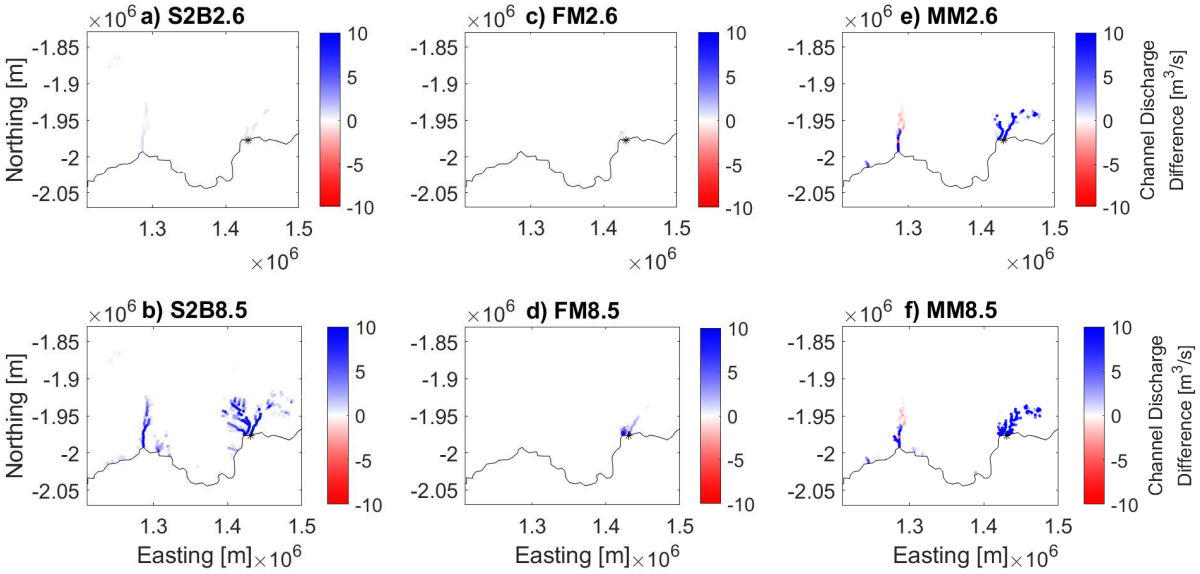

Figure 4.16: Plots of channel discharge at the end of the second year focusing on the Ninnis and Mertz Glaciers from the six future condition runs: a) S2B2.6; b) S2B8.5; c) FM2.6; d) FM8.5; e) MM2.6; and f) MM8.5. The Current run (Figure 4.13) has been subtracted from them.

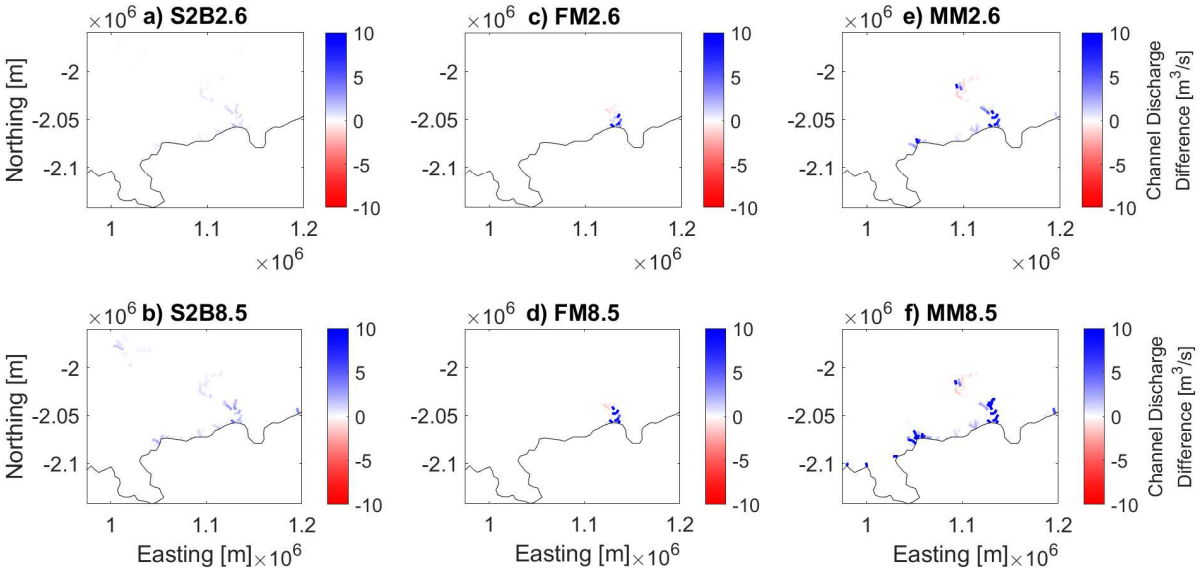

Figure 4.17: Plots of channel discharge at the peak of the second melt season focusing on the Cook Glaciers from the six future condition runs: a) S2B2.6; b) S2B8.5; c) FM2.6; d) FM8.5; e) MM2.6; and f) MM8.5. The Current run (Figure 4.13) has been subtracted from them.

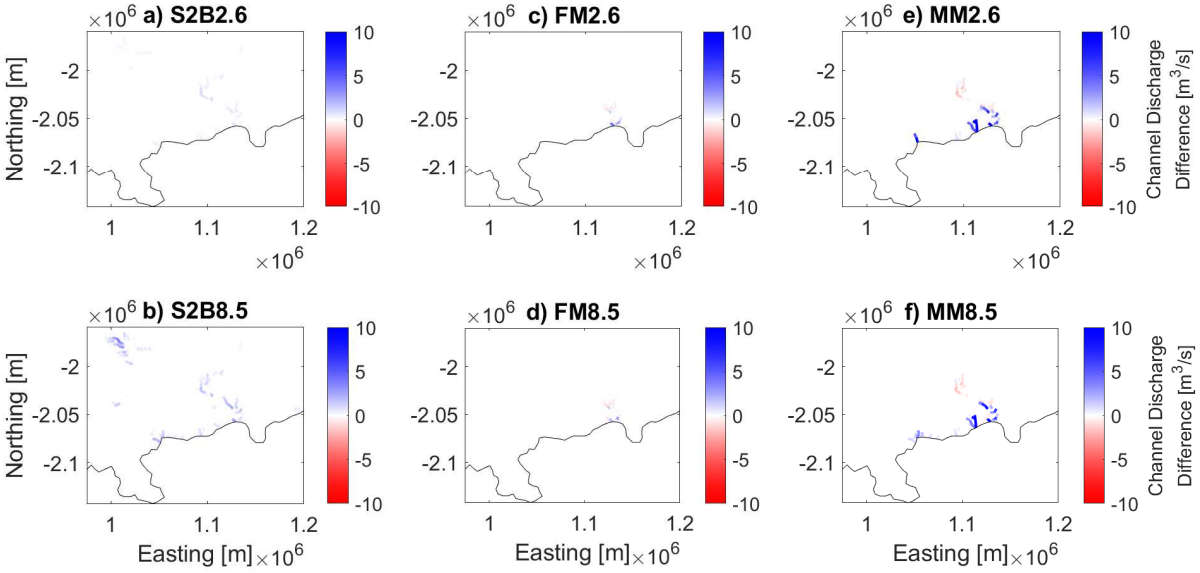

Figure 4.18: Plots of channel discharge at the end of the second year focusing on the Cook Glaciers from the six future condition runs: a) S2B2.6; b) S2B8.5; c) FM2.6; d) FM8.5; e) MM2.6; and f) MM8.5. The Current run (Figure 4.13) has been subtracted from them.

show no change in channel discharge compared to the Current run except at Cook West, where the increases mostly disappear from the peak of the second melt season (Figure 4.17c, d) to the end of the second year (Figure 4.18c, d). Both MM runs show more widespread increases in channel discharge along the grounding line, extending from Cook West to Cook East. In addition, the differences at the peak of the second melt season (Figure 4.17e, f) compared to the end of the year (Figure 4.18e, f) are mostly retained.

Chapter 5

Discussion

This discussion chapter will examine the application of the results and how they are relevant to predictions for the future of Antarctic ice sheets and ice shelves. Different methods for simplifying the transport of water from the surface to the bed are discussed first in Section 5.1. Next, Section 5.2 will compare the different predictions of moulin distribution in each future scenario and how that corresponds with the overall surface coverage of the moulin drainage basins. The reaction of Antarctic glaciers in the future might be similar to how glaciers in Greenland have changed and currently are changing, which warrants a comparison between the two regions in Section 5.3. Finally, the impact subglacial hydrology has on ice shelves is discussed in Section 5.4, as they may hold the key to the stability of the rest of the grounded ice and the whole of Antarctica.

5.1 Redirecting Supraglacial Runoff to the Subglacial Hydrology System

The goal for this project is to look at how an Antarctic subglacial hydrology system might be affected by predicted surface runoff in the year 2100. The reason for developing the moulin calculation algorithm is to try and develop a more sophisticated system to route and introduce future surface runoff into the subglacial hydrology system. A simple method that has been previously implemented assumes a heavily crevassed domain that strongly connects surface and bed hydrologies to justify water routing from where it is produced on the surface straight to the bed, like was done in the S2B scenarios (Cook et al., 2020). This assumption is not realistic in the case of the Wilkes Subglacial Basin due to the size of our domain, since crevassing should mostly be confined near the grounding line where there are higher surface velocities. However, the ease of implementation with this method makes it possible for us to use it as a point of comparison for other methods of routing surface water to the bed. The big difference between the S2B and moulin scenarios is where the surface water inputs enter the subglacial GlaDS model. The S2B scenarios input surface runoff everywhere in the domain, while the moulin scenarios only input water near the grounding line where moulins are predicted to be (Figure 4.1). This has a big effect on

the distributed drainage system model outputs with widespread increases in both water pressure (Figure 4.5) and water thickness (Figure 4.11) across the domain. This can also be seen by comparing the areas that exceed overburden pressure in each scenario. Looking at the water pressures at the peak of the second melt season, the Current run predicts that overburden pressure is reached in an area of 8.95×10^7 m^2, which is 0.015% of the domain (Figure 4.4). The moulin runs predict that overburden pressure being reached in areas covering 3.59×10^8 m^2 (0.058% of the domain), 8.68×10^9 m^2 (1.4%), 1.58×10^9 m^2 (0.23%), and 1.92×10^{10} m^2 (3.1%), for FM2.6, FM8.5, MM2.6, and MM8.5 respectively (Figure 4.5c, d, e, f). The S2B runs then predict larger areas of 4.94×10^{10} m^2 (8.1%) and 1.43×10^{11} m^2 (23%) for S2B2.6 and S2B8.5 respectively (Figure 4.5a, b). These increases from moulin to S2B scenarios do make sense as the more widespread distribution of increased water inputs lead to the distributed drainage system getting filled and pressurized. However, by inputting water throughout the entire domain, the S2B scenarios widely overestimate water pressure and water thickness compared to the moulin scenarios.

Another way surface runoff has been implemented in GlaDS before has been to use observations to position moulins for concentrated water input, alongside regions where surface runoff is sent straight to the bed (Scholzen et al., 2021). Since there is currently no surface melt nor moulins for the majority of Antarctica, we had to find a way to determine moulin positions theoretically. By having the moulin calculation algorithm be based on a variable strain threshold, we could also develop multiple scenarios with different distributions of moulins. For the most part, having more moulins (decreasing strain threshold from 0.05 to 0.01) creates more widespread differences than having a higher RCP scenario (increasing from RCP 2.6 to RCP 8.5) and correspondingly larger surface runoff rates (FM8.5 versus MM2.6 in Figures 4.5, 4.11, and 4.14). This is more likely due to the moulins in MM2.6 being more numerous and spread out than in FM8.5 (Figure 4.1) rather than the coverage of the moulin drainage basins in MM2.6 being much larger than in FM8.5 (Figure 5.1), which will be covered next. This is because the total surface runoff input into GlaDS, summed over every moulin, is still slightly larger in FM8.5 than MM2.6 (Table 4.1), purely based on the higher runoff rates in RCP 8.5. This shows that the uncertainty in the strain threshold and distribution of moulins is also important to be able to accurately model subglacial hydrology.

5.2 Moulin Formation

The first thing to note about the different moulin scenarios is that all locations are close to the grounding line of the domain (Figure 4.1). This is because the strain threshold is only surpassed near the grounding line where there are higher surface velocities and strain rates. This means that for large surface catchments, a lot of water can accumulate in the bulk of the domain clearly exceeding the accumulation threshold, but not have a moulin form since the strain threshold is only reached near the grounding line. This physically means that surface runoff builds up without ever reaching a crevasse where it can initiate hydrofracturing to create a moulin. In Greenland, moulins can be found

inland, although with decreasing density as distance from the grounding line (and surface elevation) increases. For example, Yang & Smith (2016) mapped moulins up to around 100 km inland from the grounding line, or up to elevations of 1800 m above sea level in Southwest Greenland (due to a shallower slope, similar elevations reach up to 200 km from the grounding line in the Wilkes Subglacial Basin). These moulins can also form underneath a supraglacial lake instead of in pre-existing crevasses (Hoffman et al., 2018, Clason et al., 2015). However, since we have not modelled supraglacial lake formation and drainage, they are not considered in the scope of this project.

Another thing to note about the location of the moulins is that they generally correspond to the main outlet glaciers in the Wilkes Subglacial Basin. For example, in the FM2.6 scenario (Figure 4.1a), there is a moulin near the Mertz, Ninnis, Cook, and Matusevich glaciers. This makes sense as these regions also correspond with an increased surface velocity and strain rate. The Rennick and Lillie glaciers only have moulins in the MM scenarios (Figure 4.1c, d) which means that it is not a low accumulation rate that prevents moulins from forming, but rather low strain rates in the region.

The density of moulins also increases going from RCP 2.6 to RCP 8.5 scenarios for a fixed strain threshold (Figure 4.1a to b, and c to d). This is expected, since the higher RCP scenario corresponds to larger runoff values (Figure 3.3) and so a faster build-up of surface water accumulation. The faster build-up means the accumulation threshold is more quickly surpassed which means more moulins within the same regions of high strain. We can also compare the impact between changing RCP scenarios or changing strain threshold by looking at the FM8.5 and MM2.6 scenarios. While the FM8.5 scenario predicts 19 moulins, MM2.6 predicts 31 moulins, suggesting that decreasing the strain threshold is a more impactful change than the increasing runoff rates of the RCP 8.5 scenario.

Since each moulin created has a corresponding water accumulation up to that location (which subsequently becomes the discharge into the subglacial system), we can sum the accumulation over all moulins to get the total accumulation for each scenario as shown in Table 4.1. Even though FM8.5 has a lower number of moulins than MM2.6, it has a slightly higher total accumulation. This means that each moulin must have a significantly higher discharge as shown by the fact that the average FM8.5 moulin has almost double the average accumulation rate. In fact, the FM scenarios have the highest average accumulation per moulin even comparing to their cooresponding MM scenario (with the same RCP value). While each scenario is shown as a distinct prediction of the future, the gradual changing of the real climate may mean that each of these predictions may lie on a spectrum that we could experience one at a time. This would mean that as we expect the climate to continue to warm, we could start at a scenario with fewer moulins at lower elevations near the grounding line and transition to scenarios with more moulins that are more widespread.

To learn more about the difference in total accumulation between each scenario, we can also look at the drainage basins for all the moulins (Figure 5.1). The larger drainage basins can

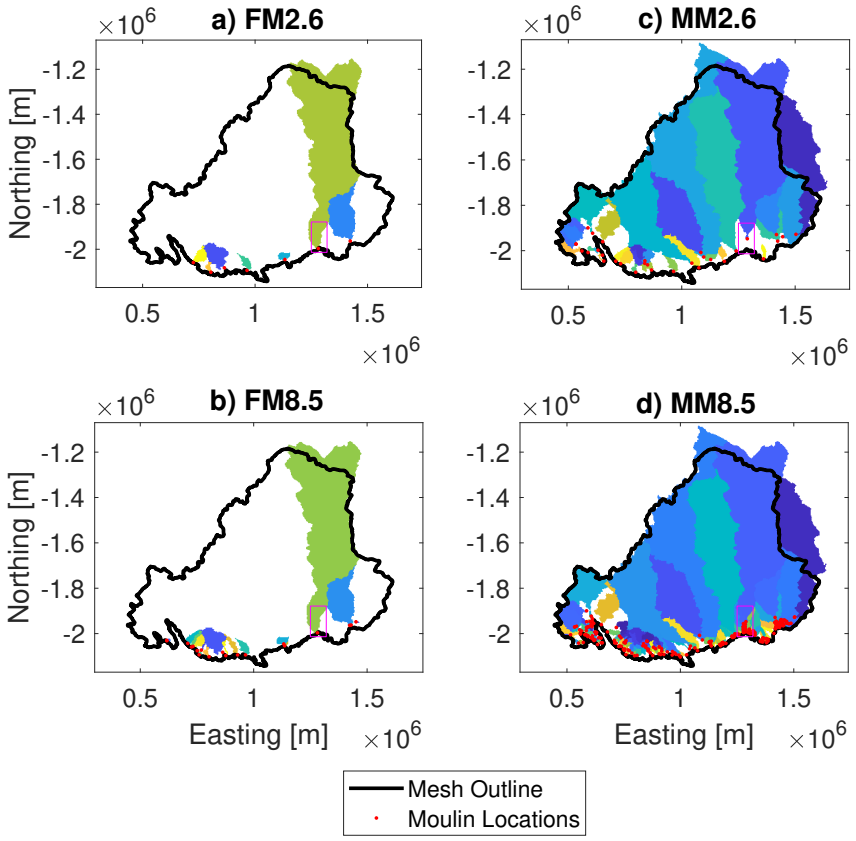

Figure 5.1: The supraglacial drainage basins for each moulin in all four moulin scenarios: a) FM2.6; b) FM8.5; c) MM2.6; and d) MM8.5. The subglacial water input calculated for each moulin is the sum of surface runoff within each corresponding drainage basin. Moulin positions are plotted as red points, while the domain boundary (based on subglacial drainage basins) is in black.

extend beyond the mesh boundaries since the surface drainage basins do not align with the subglacial drainage basins due to the difference between surface and bed topography. This means that unlike basal water, surface water produced outside the subglacial hydrology boundary can still be routed into the domain. One of the biggest differences between the moulin drainage basins from the different scenarios is that the moulin drainage basins in the FM scenarios (Figure 5.1a, b) have a significantly smaller spatial coverage than that of the MM scenarios (Figure 5.1c, d). This explains why the FM scenarios have lower total accumulations compared to their corresponding MM scenarios. The runoff produced outside of the moulin drainage basins do not contribute to moulin discharge and flows through the region without being redirected to the bed. We can also analyse the scenarios the other way by fixing the strain threshold and comparing the difference between RCP 2.6 scenarios (Figure 5.1a, c) and RCP 8.5 scenarios (Figure 5.1b, d). Although less impactful to the coverage of the moulin drainage basins, the higher RCP 8.5 scenarios create more

moulins near the grounding line that end up capturing more surface runoff.

Since there are only a few moulins in the FM2.6 scenario (Figure 5.1a), we can look at the specific drainage basins that correspond with the major outlet glaciers in the region. The two biggest moulin drainage basins in FM2.6 correspond to the moulins at Ninnis and Mertz Glaciers. The largest is the Ninnis moulin drainage basin that by itself extends vertically throughout the entire domain and sticks out near the top of the catchment. Although coloured differently, there are corresponding drainage basins that feed Ninnis Glacier in all the other scenarios as well, with only slight differences in the location of the moulin. Since the surface topography used to derive flow routing and drainage divides are the same for all scenarios, the boundary of moulin drainage basins are identical at the top of the domain. Near the grounding line, the boundary of the drainage basins are also influenced by outlet (moulin) positions. By the moulin prediction algorithm (Section 3.4), this means that the strain and runoff rates (by positioning moulins) also affects the drainage basin boundaries. Compared to the moulin at Ninnis in FM2.6 (Figure 5.1a), the moulin at Ninnis in MM2.6 (Figure 5.1c) is higher up in the catchment, which decreases the extent of the drainage basin. This higher position is directly due to the fact that the strain at that location has surpassed the MM strain threshold (0.01), but not the FM strain threshold (0.05). The rest of the area covered by the FM2.6 Ninnis drainage basin is not covered in MM2.6 (see the magenta boxed region in Figure 5.1). However, even though the MM8.5 scenario (Figure 5.1d) has the same higher moulin position as MM2.6, due to the higher RCP scenario this area near the grounding line is covered by different moulins and drainage basins. Looking at the other drainage basins in FM2.6 near Mertz and Cook (Figure 5.1a), their corresponding drainage basins in MM8.5 (Figure 5.1d) show a similar pattern where the coverage is smaller due to a higher moulin position, but the rest of the region up to the grounding line is still covered by other moulins and drainage basins. These differences in how much the moulin drainage basins cover the domain are a result of the differences in the number and position of moulins predicted in each scenario. This in turn controls changes how the magnitude and spatial distribution of runoff being introduced to the bed changes between scenarios.

5.3 Comparing the Future of Antarctica to Present Day Greenland

The picture of the future of Antarctic being painted by current climate models shows widespread temperature and surface runoff increases (Figure 3.3), similar to present day Greenland. The higher surface runoff rates mean more water in the subglacial hydrology system which will lead to higher water thicknesses that lubricate the base of the ice sheet and higher water pressures that lift the overlying ice. This will lead to increases in ice velocities, the correlation of which can also be seen in the current surface velocity and water pressures. Figure 5.2 shows a correspondence between the water pressure in the Current run and the MEaSUREs surface velocity map at Mertz, Ninnis, Cook, Matusevich, and

Rennick.

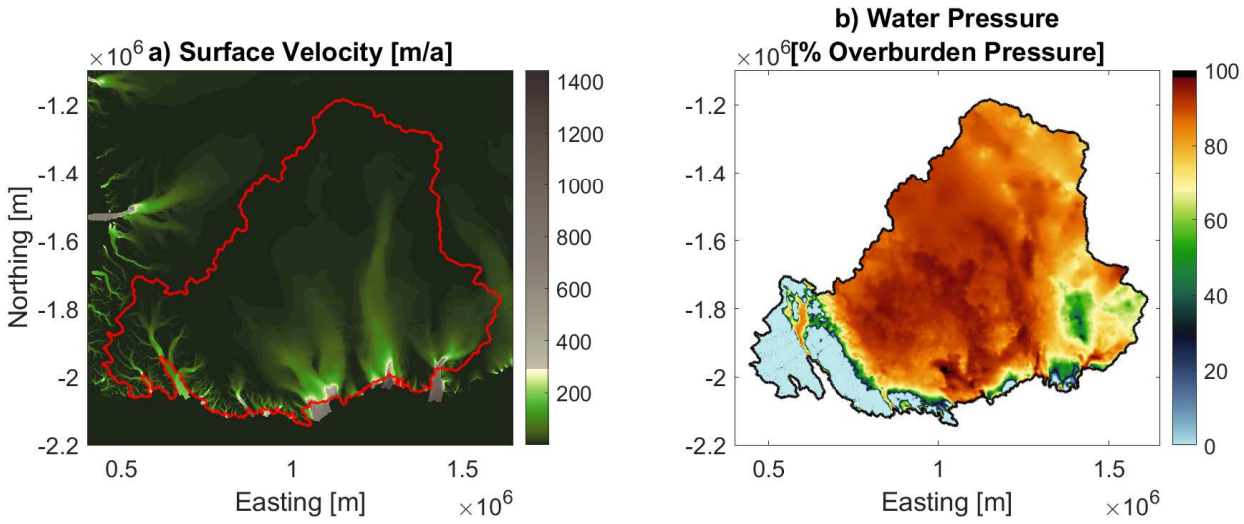

Figure 5.2: Plots to compare surface velocity and Current run water pressure in the Wilkes Subglacial Basin. a) Surface velocity comes from the MEaSUREs InSAR-based Antarctica ice velocity map, where the Wilkes Subglacial Basin region is outlined in red. b) Water pressure from the Current run, which is the same as in Figure 4.4.

The water pressure increases as predicted in the future run GlaDS outputs (Figure 4.5) will correspond to future ice velocity increases, and how they will change in space and time could be similar to how Greenlandic glaciers behave today. Moon et al. (2014) describes three different types of Greenlandic glaciers based on different annual patterns in velocity. They are suggested to come from differences in ice-front position, surface runoff availability, and subglacial drainage developments. Type 1 glaciers have a subglacial hydrology system that does not transition from inefficient to efficient over the melt season, and sees a sustained velocity increase throughout the year even after the melt season. Type 2 glaciers also do not have a subglacial hydrology system that transitions becomes channelized and efficient, but velocities are correlated with runoff. Increases are only observed during the melt season and return to pre-summer speeds once there is no more runoff. Type 3 glaciers do have a subglacial hydrology system that transitions from an inefficient to an efficient drainage system. This shows up as a significant velocity low at the end of the melt season compared to pre-summer levels.

Figure 5.3 plots average water pressure over fast flowing regions in the Wilkes Subglacial Basin. This is first done by creating regions at each outlet glacier where basal velocity exceeds 100 m/a (plotted as polygons in Figure 5.4). These fast flowing regions include the outlet node if disconnected from the fast flowing region. Then, we can average over all

nodes that are inside each fast flowing region. Since the mesh was refined based on areas with basal velocity greater than 30 m/a, the element size and distribution of nodes within each region are relatively uniform and avoids biasing based on averaging over different densities of nodes. There is an exception to this process at Lillie glacier, where there are no basal speeds that exceed 100 m/a. The water pressure plotted is only of the one outlet node. The first thing to note about Figure 5.3 is how the future scenarios compare with the Current run average water pressures. The Current run predicts water pressures consistently below 100% overburden pressure, when we expect ice uplift and faster sliding velocities from reduced basal friction (Iken & Bindschadler, 1986). The future scenarios however do start predicting that water pressure will exceed overburden pressure, especially during the melt seasons, and especially for the S2B8.5 and both MM scenarios.

These average water pressure patterns can also be used as a proxy for velocity patterns, letting us classify the different outlet glaciers into the three glacier types in Moon et al. (2014). At Mertz Glacier (Figure 5.3a), water pressure for all the RCP 8.5 scenarios (S2B8.5, FM8.5, and MM8.5) all exhibit a pattern similar to a type 2 glacier, where an increase in water pressure during the melt season is followed by a decrease once the additional surface runoff disappears for the year. These decreases don't always return back to the baseline water pressure set by the Current run, but may return to a new, higher baseline which is hard to confirm with only two melt seasons modelled. There also seems to be a second bump in average water pressure outside of the first melt season, that diminishes after the second melt season in comparison. This might be caused by lags in water flow through the subglacial hydrology as the drainage system adapts to the sudden water input in contrast to steady state. The S2B2.6 scenario at Mertz (Figure 5.3a) has a different average water pressure behaviour that just steadily increases regardless of melt season or not, which is also observed at some glaciers in Greenland for some years by Moon et al. (2014). The pattern at Rennick Glacier (Figure 5.3e) is similar to Mertz (noting the difference in the scale of average water pressure), showing type 2 behaviour for all RCP8.5 scenarios (besides FM8.5 this time), and an anomalous secondary peak after the first melt season. The S2B2.6 similarly shows the pattern of steady increase regardless of melt season.

Ninnis and Cook West Glaciers (Figure 5.3b, c) display a slightly different average water pressure pattern, where both MM2.6 and MM8.5 show a slight decrease in water pressure compared to the Current run, indicative of a type 3 glacier. This is corroborated by significant channelization at Ninnis and Cook for the MM scenarios (Figures 4.15 and 4.17), suggesting that the subglacial hydrology system has transitioned from an inefficient system to a channelized, efficient mode. However, Ninnis Glacier for scenario S2B8.5, along with Mertz Glacier for most scenarios, show channelization while the average water pressure does not decrease enough to dip below the Current pressure. This suggests that type 2 glaciers may also develop an efficient subglacial drainage system without a significant decrease in water pressure.

Matusevich Glacier has the clearest case of a type 1 glacier in these model runs. S2B2.6 and S2B8.5 at Matusevich Glacier show a ramp up in water pressure during the first melt

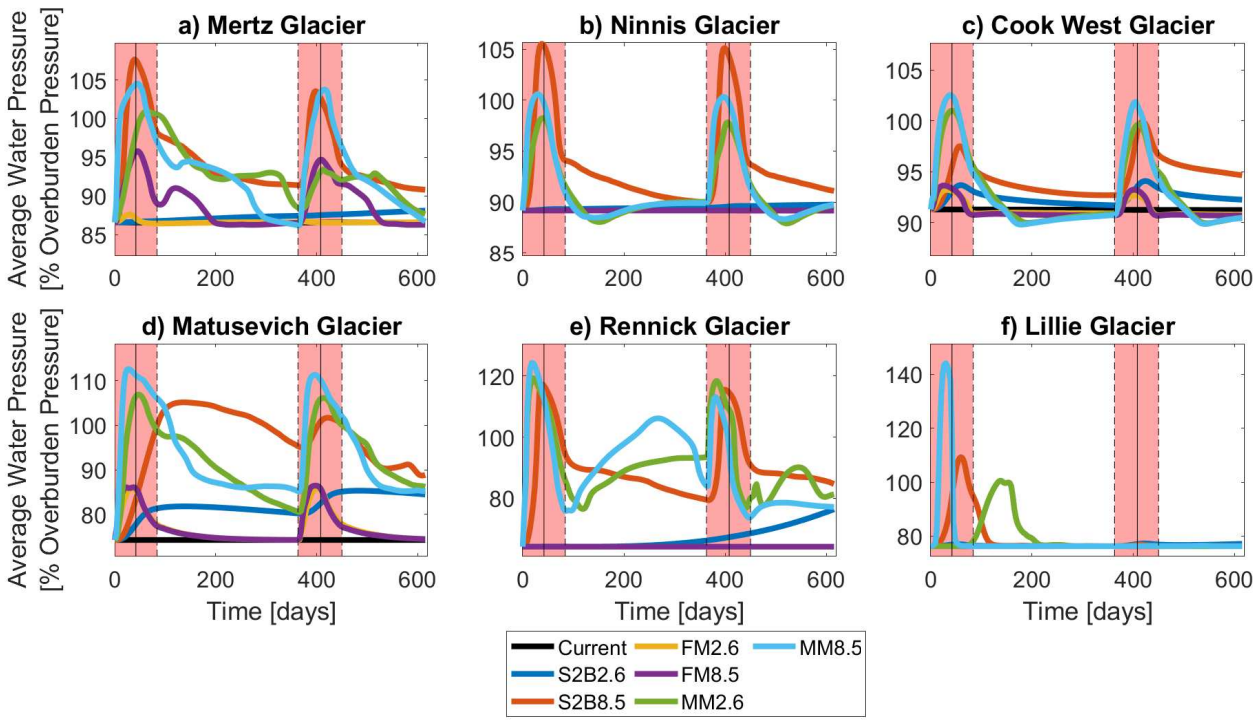

Figure 5.3: Plots of average water pressure for every transient run over time in the fast flowing (basal velocity greater than 100 m/a) regions of each outlet glacier: a) Mertz; b) Ninnis; c) Cook West; d) Matusevich; e) Rennick; and f) Lillie Glaciers. The extents where each outlet glacier is considered fast flowing are plotted as polygons in Figure 5.4. The two melt seasons are highlighted by a red background along with vertical dashed and solid lines indicating the start, stop, and peak. Note the different scales in y-axis for each different glacier.

season that remains high with only slight decrease over winter. After the second melt season this is not as clear for S2B8.5, but S2B2.6 still seems to exhibit a type 1 glacier pattern.

Lillie Glacier has an interesting feature where MM8.5, MM2.6, and S2B8.5 show a type 2 pattern during the first melt season, but all scenarios show no more change in water pressure during the second melt season. This could be due to the fact that we are only plotting a single node (as the Lillie Glacier catchment does not exceed 100 m/a basal velocity anywhere), and the subglacial hydrology system has developed in a way that stop routing water to our plotted node.

It has been observed in Greenland that there is no strict relationship between total surface runoff and the total ice discharge, calculated as the mass of ice crossing the grounding line and becoming part of the floating ice shelf (King et al., 2018). Comparing different years between 2000-2016 in Greenland, some years with higher surface melt and runoff happen to discharge less ice (instead of more). From our results, one possible reason for the lack

of positive correlation could be due to differences in moulin position and density which we have shown may have a larger impact on subglacial hydrology than surface runoff. Specifically, we do see larger and more widespread water pressure increases at the peak of a melt season in MM2.6 (with a lower total surface water input) than FM8.5 (Figures 4.8 and 4.9 respectively). This could suggest a larger speed-up in MM2.6 than FM8.5 due to higher water pressures, resulting in a higher ice discharge.

That being said, between each method of surface water input and strain threshold (S2B, FM, and MM), the RCP 8.5 scenarios always shows more differences in GlaDS outputs than their corresponding RCP 2.6 scenarios. The larger volumes of water being input into the subglacial hydrology system means larger water thicknesses filling cavities, more widespread water pressure increases that lift overlying ice, and more channels with larger channel discharge rates. This is important because it shows the impact of taking more action to emit less greenhouse gases into the atmosphere to lower which RCP scenario we are headed toward.

When it comes to the channel discharge (Figure 4.14), the S2B scenarios predict a spatial distribution very similar to that of the moulin scenarios, specifically between the S2B8.5 and MM8.5 outputs. Unlike the water pressure and water thickness, the S2B scenarios only differ from the Current run near the grounding line. This shows that even though a lot of water was input outside of the grounding line in the S2B scenarios, channels still couldn't form there. However, there is a big difference in channel discharge between S2B2.6 and S2B8.5 that is not as prominent in the moulin scenarios. While S2B8.5 shows large differences in channel discharge at Mertz, Ninnis, and Matusevich Glaciers, S2B2.6 shows almost no difference from the Current run anywhere. In the moulin runs, the RCP 2.6 scenarios still show channelization in some regions, which are increased in the corresponding RCP 8.5 scenarios. This shows that in the RCP 2.6 scenario, the concentrated water inputs through moulins seems to be better at creating channels than the widespread water inputs in the S2B2.6 scenario sent straight to the bed, which still needs to traverse through and accumulate in the subglacial hydrology system.

5.4 The Impact of Subglacial Hydrology on the Future of Antarctic Ice Shelves

Looking at the spatial distribution of channel discharge, we can also examine how often out of all the scenarios that each outlet glacier has channels. The Current run only has channels forming at Mertz, Ninnis, and the Cook Glaciers (Figure 4.13). While S2B2.6 again has no significant change in channelization from the Current run, both FM scenarios have small increases in channel discharge at Mertz and Cook West Glacier, along with new channel discharge at Matusevich Glacier. The rest of the three scenarios, S2B8.5 and both MM scenarios, also have increased channel discharges at Mertz, Cook West, and Matusevich, along with Ninnis, Cook East, Rennick, and Lillie Glaciers (Figure 4.14).

Knowing the likely locations of current and future channelization in the region is important when considering the impact that localized discharge may have on melting below ice shelves.

Subglacial hydrology can affect ice shelves by causing melt due to subglacial discharge over the grounding line. When the subglacial discharge is highly localized as at the outlet of a subglacial channel over the grounding line, the introduction of freshwater can increase turbulent heat transfer as it rises along the base of the ice shelf. This then increases melting along a path from the outlet, and can cause basal channels (underneath the ice shelves) to form. Basal channels then have been found to lead to tranverse fractures that could cause subsequent calving and loss of ice based along the initial fracture (Dow et al., 2018b).

Alley et al., (2016) used satellite and airborne radar data to find and classify ice shelf basal channels across Antarctica. The three basal channel classifications they used included: ocean-sourced for channels that appear away from the grounding line, grounding line-sourced for channels that reach the grounding line where there is no predicted discharge, and subglacially-sourced for channels found intersecting where there is predicted discharge over the grounding line. The only basal channels they documented are in the Wilkes Subglacial Basin at Rennick and Lillie Ice Shelves, with 184 km and 60 km of total channel length respectively. Both Rennick and Lillie Glaciers do not see significant subglacial channelization in the Current run (Figure 4.13), which agrees with the fact that they are only classified as ocean- and grounding line-sourced, and not subglacially-sourced. However, this also leaves the fact that no ice shelf basal channels were found at the Mertz, Ninnis, and Cook West Glaciers where we do see subglacial channelization. If these outlet glaciers were just overlooked in the Antarctic-wide analysis, it will be a good exercise to directly compare current surface elevation of the ice shelves where GlaDS predicts the highest channel discharge over the grounding line.

Wei et al. (2020) has shown that there is a possible connection between the location of predicted subglacial channel outlets and the location of higher ice shelf melt rates near the grounding line. These higher melt rates are also independent of there being ice shelf basal channels. So, predicted locations of increased subglacial channelization at the grounding line may be tracked to be able to correlate with increased ice shelf basal melt rates nearby (Le Brocq et al., 2013). This is where subglacial hydrology may be able to play another role in the evolution of the Antarctic ice sheet, in addition to the traditional way of increasing water pressure and ice lift reducing basal friction (Iken & Bindschadler, 1986). This is because increased ice shelf melting can decrease the buttressing force as ice shelves thin, which will be interesting to track to determine if they further lead to acceleration of grounded ice and contribution to sea level rise (Fürst et al., 2016).

Adusumilli et al. (2020) used changes in velocity and surface height of Antarctic ice shelves to predict the spatial distribution of basal melt rates. This is plotted on top of the Current run channel discharge in Figure 5.4. Ice shelf basal melt rates were only found on Mertz, Cook, and Rennick Ice Shelves, which corresponds poorly with the channelization found in

the Current model run. One instance is at Rennick Glacier where there is no channelization in the Current run while there is ice shelf basal melt. The other instance is at Cook, where ice shelf basal melt rates show a spike on the east side of the Cook Ice Shelf, while the GlaDS run only shows subglacial channelization at Cook West. The reasons for these discrepancies could be due to the methodology like mesh resolution at the important outlet or having important constants like sheet and channel conductivity be constant throughout the entire domain. More fundamentally, this mismatch between subglacial channels and ice shelf melt rate could also be due to lack of data in the Adusumilli map, or errors in the BedMachine Antarctica basal topography of the region which has a large control on subglacial hydrology. We have also seen that the GlaDS model has trouble around Rennick Glacier since it is near the Transantarctic Mountains with very high elevations and zero ice thickness. In any case, due to the sensitivity of outputs like water pressure and channelization on moulin distribution and RCP scenario, it will be extremely important to figure out the reason for this mismatch to be able to better corroborate future predictions in the region.

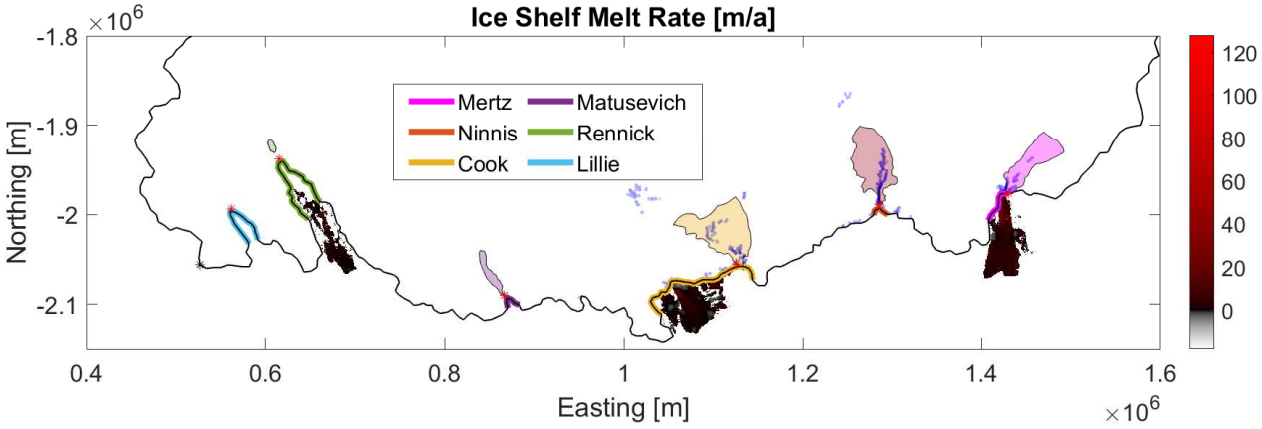

Figure 5.4: Plot of ice shelf melt rates from Adusumilli et al. (2020). Includes the Current run channel discharge which is the same as in Figure 4.13. The extent of grounding line used to calculate total subglacial discharge at each outlet glacier in Figure 5.5 is highlighted in their respective colours. Also plotted is the portion of the catchment of each outlet glacier where basal velocity is higher than 100 m/a used to calculate average water pressures previously shown in Figure 5.3. The position of the outlet used to calculate glacier catchments are plotted as red stars.

While the Current run channelization corresponds poorly to current data about ice shelf basal channels and basal melt rate, we can still look at how channel discharge over the grounding line will change in the future. Figure 5.5 plots cumulative channel discharge over the grounding line for all transient runs, broken down by outlet glacier. First, each outlet glacier was defined an extent of the grounding line that they covered, which is plotted in Figure 5.4. Then, the channel discharge that flows into each of the corresponding grounding line extents were summed and plotted over time.

Each future scenario sees different glaciers dominate in total grounding line channel discharge, while there are also completely different orders of magnitude of maximum channel discharge (noting the changing channel discharge scales on the y-axis). The cumulative grounding line discharge in the S2B2.6 scenario (Figure 5.5a) shows only a slight difference from the Current, constant discharge (plotted as dashed lines). The S2B8.5 scenario (Figure 5.5b) sees an order of magnitude increase in maximum grounding line discharge, with all outlet glaciers experiencing increases. There is also an interesting behaviour at Mertz between the first and second year. After the first melt season, the channel discharge remains steady between melt seasons before increasing again at the second melt season. This could be due to the nature of the S2B scenarios and how water is input even at the top of the domain. Instead of seeing decreasing channel discharge when surface water inputs stop, the water that was input further up the domain lags while flowing through the subglacial hydrology system before reaching the grounding line between melt seasons. This delay also makes it so that there is only enough water to pressurize the system and form channels at the second melt season, which makes the cumulative channel discharge at the second melt season significantly greater than the first.

The FM2.6 and FM8.5 scenarios (Figure 5.5c, d) have total grounding line discharge dominated by the Mertz and Matusevich regions, and we again see the maximum channel discharges jump an order of magnitude between RCP 2.6 and 8.5 scenarios. This is repeated again with MM2.6 and MM8.5 (Figure 5.5e, f). These predicted channel discharge rates of over thousands of cubic metres per second are likely too large to be physically possible. One of the reasons for this could be the simplicity in flow routing calculation used to determine moulin discharge rates. By assuming all melt water in a catchment will make it to the moulin regardless of distance and timing does make the predicted moulin discharge rates an upper bound if no melt water water enters a terminal supraglacial lake or refreezing in a firn aquifer along the way. However, the differences in the magnitude of grounding line discharge between the future scenarios does correspond with the changes in total moulin accumulation in the domain (Table 4.1). This could also point to a problem with the climate models predicting unreasonably large runoff rates over specific areas of the domain (Figure 3.3). This would probably require more improvements to how global climate models predict the future in Antarctica, or else make it necessary to use more focused regional climate models. This again shows how important each component is, from runoff rates to moulin distribution and regional topography, to be able to predict how the subglacial hydrology system will develop in the future.

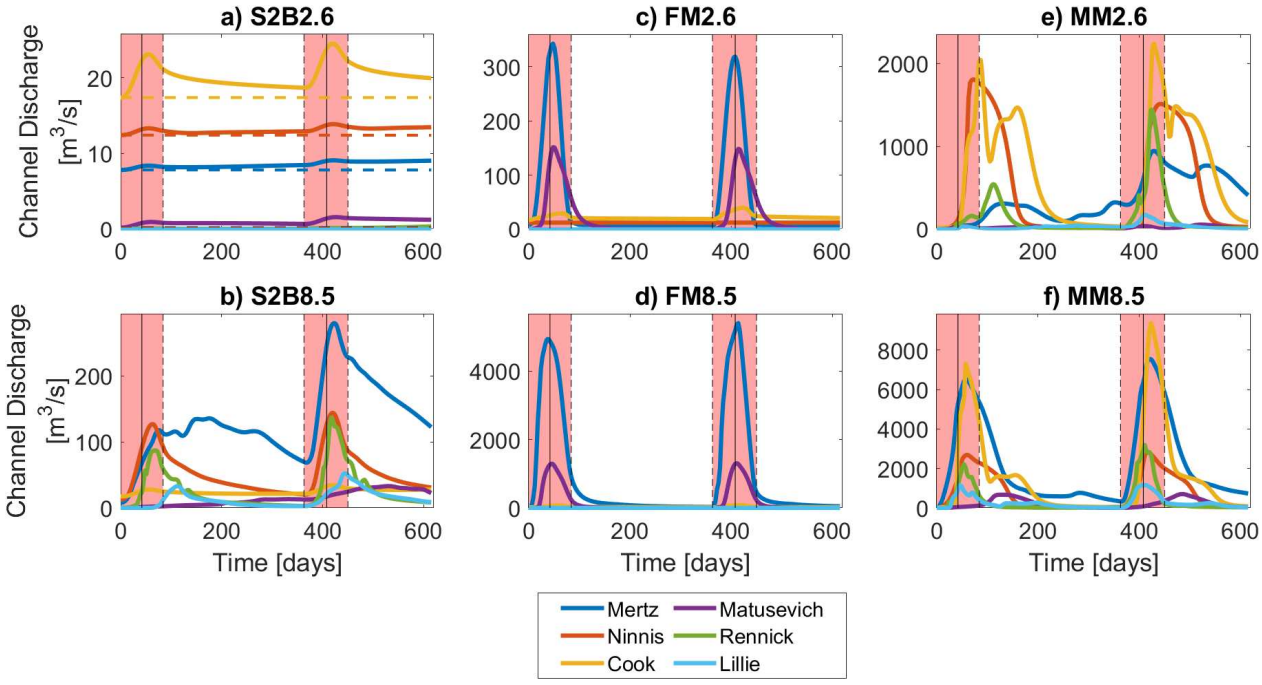

Figure 5.5: Plots of the total channel discharge flowing into the grounding line at each outlet glacier over time for all transient runs: a) S2B2.6 (solid) and Current (dashed); b) S2B8.5; c) FM2.6; d) FM8.5; e) MM2.6; and f) MM8.5. The extent of the grounding line at each glacier over which discharge is summed is shown in Figure 5.4 using the same colours for each glacier. The two melt seasons are highlighted by a red background along with vertical dashed and solid lines indicating the start, stop, and peak. Note the different scales in y-axis for each different model run.

Chapter 6

Conclusion

We now conclude the thesis by first providing a summary of the project and thesis, before considering limitations of the project and what improvements or next steps can be taken in the future.

6.1 Summary

The goal of this project was to model the future state of the subglacial hydrology system in the Wilkes Subglacial Basin using climate model predictions of surface runoff. All other subglacial hydrology parameters including topography, ice thickness, and velocities was taken from datasets of the current state of the Antarctic. The surface mass balance (SMB) runoff predictions for the year 2100 was taken from the CCSM4 climate model and introduced into the GlaDS model in six different future scenarios. These scenarios are all combinations between two different representative concentration pathway (RCP) scenarios, RCP 2.6 and 8.5, and three difference surface input methods, sending surface water straight to the bed (S2B), and fewer and more moulin scenarios (FM and MM). Future moulin distributions for the moulin scenarios were calculated using an algorithm based on thresholds for strain and accumulation rate used as proxies for the process of hydrofracturing.

GlaDS model outputs for the S2B scenarios show catchment-wide increases in the water pressure and water thickness compared to the Current run without surface water input, but not for channel discharge. This makes sense as water is input into the distributed drainage system throughout the entire catchment, which heavily changes the distributed drainage system parameters. This shows the limitations of assuming water can be sent straight to the bed in most of Antarctica. The moulin scenarios show changes constrained near the grounding line, due to surface water throughout the domain being automatically transferred to moulins which are only located near the grounding line. These show a more realistic subglacial hydrology system, where water pressure changes and channelization are most prominent near the outlet glaciers found near basal troughs and ice streams.

Comparing the FM8.5 and MM2.6 scenarios is used as a shorthand for comparing the impacts between independently increasing the RCP scenario or increasing the number of moulins. This comparison shows MM2.6 having a wider impact on all system parameters compared to FM8.5, and means that moulin placement and distribution is more important than RCP scenario when it comes to the subglacial hydrology system in the Wilkes Subglacial Basin. Despite this, the higher RCP 8.5 scenario did have a larger impact for each surface input method (S2B, FM, MM) compared to the RCP 2.6 scenario with no exceptions. This shows that both moulin distribution and RCP scenario are both important in determining the future of the subglacial hydrology system in the region. Further, they will also impact ice shelf-ocean interactions and ice sheet dynamics with potential impacts that will be felt around the world. This makes it important to keep refining and improving our knowledge and methods to be able to more accurately predict what's in store for our collective futures.

6.2 Limitations and Next Steps

One of the first possible improvements that comes to mind is to expand the scope and model more physical systems. Although the project is described as modelling the future, the only data we have projected to the future to justify this is surface runoff. The rest of the parameters we used to model Wilkes Subglacial Basin are not only taken from recent observations, but are kept temporally constant throughout the model run. An ideal model setup would be able to couple the subglacial hydrology model to other domains like ice sheet, ice shelf, and ocean models to be able to simulate dynamics in the larger physical system. More realistically for the near future, a smaller step would be to change one or two more of our parameters to be projected in time. Interesting and important parameters to consider would be the future evolution of basal melt, basal velocity, surface stress and strain rates, ice thickness, and grounding line position.

One of the main contributions of this project is a new way to position moulins based on the spatial distribution of surface runoff and surface strain rates. While the simple threshold based approach was able to provide a good range of moulin scenarios to choose from only a few input variables, a lot of simplifications were made to fracture mechanics and supraglacial hydrology. Work still needs to be done to determine the impact these simplifications may have on subglacial hydrology. Just based on the differences between the fewer and more moulin scenarios though, we have shown that changing position and distribution of moulins makes a big impact to subglacial hydrology. One interesting way to make the fracture calculations more realistic could be to train and use neural networks as was done in Lai et al., (2020) to determine fractures on ice shelves from satellite images. Lai et al. also used linear elastic fracture mechanics theory to calculate the stability of fractures if they would be inundated with meltwater. Once moulins are positioned, a more realistic way to determine the water accumulation that reaches each moulin could be achieved using a supraglacial hydrology model like the Subaerial Drainage System (SaDS) model, which is similar in concept to the GlaDS model (Hill & Dow, 2021). These changes

show how the moulin and surface water input predictions can be more sophisticated and make fewer simplifications.

In addition to improving this model setup, it would also be interesting to apply this modelling project more widely to more regions around Antarctica. Due to the uniqueness of many regions in Antarctica based on topography and ice sheet and shelf geometry for example, it would be interesting to perform a wider study of general patterns in subglacial hydrology response to future surface water inputs. Changes in temporal parameters can also be investigated, from adding daily fluctuations to the melt season factor (Figure 3.6), to increasing the length of the model run times to encompass more years and melt seasons. Performing model runs with more melt seasons could also allow for scenarios that start with no annual surface water input and slowly interpolate and ramp up surface runoff every melt season until the projected values for the year 2100. Gradual temporal changes like this in a model run will make it possible to have continuous moulin formation and channel discharge values that may better match the changes we may experience as we approach the year 2100. All of these possible changes and improvements would be to try and obtain better predictions of the future state of the subglacial hydrology system. More work needs to be done, but to be able to prepare for a changing climate and rising sea levels, we will need to learn more about the complex interplay between ice, water, and land in the southern continent.

References

Adusumilli, S., Fricker, H. A., Medley, B., Padman, L., and Siegfried, M. R. (2020). Interannual variations in meltwater input to the Southern Ocean from Antarctic ice shelves. *Nature Geoscience*, 13, 616–620. https://doi.org/10.1038/s41561-020-0616-z

Alley, K., Scambos, T., Siegfried, M., and Fricker, H. A. (2016). Impacts of warm water on Antarctic ice shelf stability through basal channel formation. *Nature Geoscience*, 9, 290–293. https://doi.org/10.1038/ngeo2675

Barthel, A., Agosta, C., Little, C. M., Hattermann, T., Jourdain, N. C., Goelzer, H., Nowicki, S., Seroussi, H., Straneo, F., and Bracegirdle, T. J. (2020). CMIP5 model selection for ISMIP6 ice sheet model forcing: Greenland and Antarctica, *The Cryosphere*, 14, 855–879. https://doi.org/10.5194/tc-14-855-2020

Benn, D. I., and Evans, D. J. A. (2013). Glaciers & glaciation (2nd ed). *Routledge*.

Chu, W., Schroeder, D. M., and Siegfried, M. R. (2018). Retrieval of englacial firn aquifer thickness from ice-penetrating radar sounding in Southeastern Greenland. *Geophysical Research Letters*, 45, 11770–11778. https://doi.org/10.1029/2018GL079751

Clason, C. C., Mair, D. W. F., Nienow, P. W., Bartholomew, I. D., Sole, A., Palmer, S., and Schwanghart, W. (2015). Modelling the transfer of supraglacial meltwater to the bed of Leverett Glacier, Southwest Greenland. *The Cryosphere*, 9, 123–138. https://doi.org/10.5194/tc-9-123-2015

Collins, M., R. Knutti, J. Arblaster, J.-L. Dufresne, T. Fichefet, P. Friedlingstein, X. Gao, W. J. Gutowski, T. Johns, G. Krinner, M. Shongwe, C. Tebaldi, A. J. Weaver and M. Wehner, (2013). Long-term climate change: projections, commitments and irreversibility. In: Climate *Change 2013: The Physical Science Basis. Contribution of Working Group I to the Fifth Assessment Report of the Intergovernmental Panel on Climate Change* [Stocker, T.F., D. Qin, G.-K. Plattner, M. Tignor, S.K. Allen, J. Boschung, A. Nauels, Y. Xia, V. Bex and P.M. Midgley (eds.)]. *Cambridge University Press*, Cambridge, United Kingdom and New York, NY, USA.

Cook, S. J., Christoffersen, P., Todd, J., Slater, D., and Chauché, N. (2020). Coupled modelling of subglacial hydrology and calving-front melting at Store Glacier, West Greenland. *The Cryosphere,* 14(3), 905–924. https://doi.org/10.5194/tc-14-905-2020

Creyts, T. T., and Schoof, C. G. (2009). Drainage through subglacial water sheets. *Journal of Geophysical Research*, 114(F4), F04008. https://doi.org/10.1029/2008JF001215

Cuffey, K., and Paterson, W. S. B. (2010). The physics of glaciers (4th ed). *Elsevier.*

Das, S. B., Joughin, I., Behn, M. D., Howat, I. M., King, M. A., Lizarralde, D., and Bhatia, M. P. (2008). Fracture propagation to the base of the Greenland ice sheet during supraglacial lake drainage. *Science*, 320, 778–781. https://doi.org/10.1126/science.1153360

de Fleurian, B., Werder, M. A., Beyer, S., Brinkerhoff, D. J., Delaney, I., Dow, C. F., Downs, J., Gagliardini, O., Hoffman, M. J., Hooke, R. L., Seguinot, J., and Sommers, A. N. (2018). SHMIP the subglacial hydrology model intercomparison project. *Journal of Glaciology*, 64(248), 897–916. https://doi.org/10.1017/jog.2018.78

Dow, C. F., Werder, M. A., Babonis, G., Nowicki, S., Walker, R. T., Csatho, B., and Morlighem, M. (2018a). Dynamics of active subglacial lakes in Recovery Ice Stream. *Journal of Geophysical Research: Earth Surface,* 123(4), 837–850. https://doi.org/10.1002/2017JF004409

Dow, C. F., Lee, W. S., Greenbaum, J. S., Greene, C. A., Blankenship, D. D., Poinar, K., Forrest, A. L., Young, D. A., and Zappa, C. J. (2018b). Basal channels drive active surface hydrology and transverse ice shelf fracture. *Science Advances*, 4(6), eaao7212. https://doi.org/10.1126/sciadv.aao7212

Dow, C. F., McCormack, F. S., Young, D. A., Greenbaum, J. S., Roberts, J. L., and Blankenship, D. D. (2020). Totten Glacier subglacial hydrology determined from geophysics and modeling. *Earth and Planetary Science Letters*, 531, 115961. https://doi.org/10.1016/j.epsl.2019.115961

Flowers, G. E. (2015). Modelling water flow under glaciers and ice sheets. *Proceedings of the Royal Society A: Mathematical, Physical and Engineering Sciences*, 471(2176), 20140907. https://doi.org/10.1098/rspa.2014.0907

Fountain, A. G., and Walder, J. S. (1998). Water flow through temperate glaciers. *Reviews of Geophysics*, 36(3), 299–328. https://doi.org/10.1029/97RG03579

Fürst, J., Durand, G., Gillet-Chaulet, F., Tavard, L., Rankl, M., Braun, M., and Gagliardini, O. (2016). The safety band of Antarctic ice shelves. *Nature Climate Change*, 6, 479–482.

https://doi.org/10.1038/nclimate2912

Ge, M., Friedrich, J., and Vigna, L. (2020). 4 charts explain greenhouse gas emissions by countries and sectors. *World Resources Institute*. Retrieved from: https://www.wri.org/insights/4-charts-explain-greenhouse-gas-emissions-countries-and-sectors

Hill, T., and Dow, C. F. (2021). Modeling the dynamics of supraglacial rivers and distributed meltwater flow with the Subaerial Drainage System (SaDS) model. *Journal of Geophysical Research: Earth Surface*, 126, e2021JF006309. https://doi.org/10.1029/2021JF006309

Hoffman, M. J., Perego, M., Andrews, L. C., Price, S. F., Neumann, T. A., Johnson, J. V., Catania, G., and Lüthi M. P. (2018). Widespread moulin formation during supraglacial lake drainages in Greenland. *Geophysical Research Letters*, 45, 778–788. https://doi.org/10.1002/2017GL075659

Iken, A. (1981). The effect of the subglacial water pressure on the sliding velocity of a glacier in an idealized numerical model. *Journal of Glaciology*, 27(97), 407-421. https://doi.org/10.3189/S0022143000011448

Iken, A. and Bindschadler, R. A. (1986). Combined measurements of subglacial water pressure and surface velocity of Findelengletscher, Switzerland: conclusions about drainage system and sliding mechanism. *Journal of Glaciology*, 32(110), 101–119. https://doi.org/10.3189/S0022143000006936

King, M. D., Howat, I. M., Jeong, S., Noh, M. J., Wouters, B., Noël, B., and van den Broeke, M. R. (2018). Seasonal to decadal variability in ice discharge from the Greenland Ice Sheet, *The Cryosphere*, 12, 3813–3825. https://doi.org/10.5194/tc-12-3813-2018

Lai, C.-Y., Kingslake, J., Wearing, M. G., Chen, P.-H. C., Gentine, P., Li, H., and van Wessem, J. M. (2020). Vulnerability of Antarctica's ice shelves to meltwater-driven fracture. *Nature*, 584, 574–578. https://doi.org/10.1038/s41586-020-2627-8

Le Brocq, A. M., Ross, N., Griggs, J. A., Bingham, R. G., Corr, H. F. J., Ferraccioli, F., Jenkins, A., Jordan, T. A., Payne, A. J., Rippin, D. M., and Siegert, M. J. (2013). Evidence from ice shelves for channelized meltwater flow beneath the Antarctic Ice Sheet. *Nature Geoscience*, 6(11), 945–948. https://doi.org/10.1038/ngeo1977

Martín-Español, A., Zammit-Mangion, A., Clarke, P. J., Flament, T., Helm, V., King, M. A., Luthcke, S. B., Petrie, E., Rémy, F., Schön, N., Wouters, B., and Bamber, J. L. (2016). Spatial and temporal Antarctic Ice Sheet mass trends, glacio-isostatic

adjustment, and surface processes from a joint inversion of satellite altimeter, gravity, and GPS data. *Journal of Geophysical Research: Earth Surface*, 121, 182–200. https://doi.org/10.1002/2015JF003550

Mengel, M., Nauels, A., Rogelj, J., and Schleussner, C.-F. (2018). Committed sea-level rise under the Paris Agreement and the legacy of delayed mitigation action. *Nature Communications*, 9, 601. https://doi.org/10.1038/s41467-018-02985-8

Meredith, M., M. Sommerkorn, S. Cassotta, C. Derksen, A. Ekaykin, A. Hollowed, G. Kofinas, A. Mackintosh, J. Melbourne-Thomas, M. M. C. Muelbert, G. Ottersen, H. Pritchard, and E. A. G. Schuur (2019). Polar regions. In: *IPCC Special Report on the Ocean and Cryosphere in a Changing Climate* [H.-O. Pörtner, D.C. Roberts, V. Masson-Delmotte, P. Zhai, M. Tignor, E. Poloczanska, K. Mintenbeck, A. Alegría, M. Nicolai, A. Okem, J. Petzold, B. Rama, N.M. Weyer (eds.)]. *Cambridge University Press*, Cambridge, UK and New York, NY, USA, pp. 203–320. https://doi.org/10.1017/9781009157964.005

Moon, T., Joughin, I., Smith, B., van den Broeke, M. R., van de Berg, W. J., Noël, B., and Usher, M. (2014). Distinct patterns of seasonal Greenland glacier velocity. *Geophysical Research Letters*, 41, 7209–7216. https://doi.org/10.1002/2014GL061836

Morlighem, M., Rignot, E., Binder, T., Blankenship, D., Drews, R., Eagles, G., Eisen, O., Ferraccioli, F., Forsberg, R., Fretwell, P., Goel, V., Greenbaum, J. S., Gudmundsson, H., Guo, J., Helm, V., Hofstede, C., Howat, I., Humbert, A., Jokat, W., Karlsson, N. B., Lee, W. S., Matsuoka, K., Millan, R., Mouginot, J., Paden, J., Pattyn, F., Roberts, J., Rosier, S., Ruppel, A., Seroussi, H., Smith, E. C., Steinhage, D., Sun, B., van den Broeke, M. R., van Ommen, T. D., van Wessem, M., and Young, D. A. (2020). Deep glacial troughs and stabilizing ridges unveiled beneath the margins of the Antarctic ice sheet. *Nature Geoscience*, 13, 132–137. https://doi.org/10.1038/s41561-019-0510-8

Mouginot, J., Rignot, E., Bjørk, A. A., van den Broeke, M., Millan, R., Morlighem, M., Noël, B., Scheuchl, B., and Wood, M. (2019). Forty-six years of Greenland Ice Sheet mass balance from 1972 to 2018. *Proceedings of the National Academy of Sciences*, 116 (19), 9239–9244. https://doi.org/10.1073/pnas.1904242116

Oppenheimer, M., B. C. Glavovic, J. Hinkel, R. van de Wal, A. K. Magnan, A. Abd-Elgawad, R. Cai, M. Cifuentes-Jara, R. M. DeConto, T. Ghosh, J. Hay, F. Isla, B. Marzeion, B. Meyssignac, and Z. Sebesvari (2019). Sea level rise and implications for low-lying islands, coasts and communities. In: *IPCC Special Report on the Ocean and Cryosphere in a Changing Climate* [H.-O. Pörtner, D.C. Roberts, V. Masson-Delmotte, P. Zhai, M. Tignor, E. Poloczanska, K. Mintenbeck, A. Alegría, M. Nicolai, A. Okem, J. Petzold, B. Rama, N.M. Weyer (eds.)]. https://doi.org/10.1017/9781009157964.006

Poinar, K., Dow, C. F., and Andrews, L. C. (2019). Long-term support of an active subglacial hydrologic system in southeast Greenland by firn aquifers. *Geophysical Research Letters,* 46(9), 4772–4781. https://doi.org/10.1029/2019GL082786

Ritchie, H., Roser, M., and Rosado, P. (2020). CO_2 and greenhouse gas emissions. *Published online at OurWorldInData.org.* Retrieved from: https://ourworldindata.org/co2-and-other-greenhouse-gas-emissions [Online Resource]

Röthlisberger, H. (1972). Water pressure in intra- and subglacial channels. *Journal of Glaciology*, 11(62), 177-203. https://doi.org/10.3189/S0022143000022188

Schoof, C. (2010). Ice-sheet acceleration driven by melt supply variability. *Nature,* 468(7325), 803–806. https://doi.org/10.1038/nature09618

Seroussi, H., Nowicki, S., Payne, A. J., Goelzer, H., Lipscomb, W. H., Abe-Ouchi, A., Agosta, C., Albrecht, T., Asay-Davis, X., Barthel, A., Calov, R., Cullather, R., Dumas, C., Galton-Fenzi, B. K., Gladstone, R., Golledge, N. R., Gregory, J. M., Greve, R., Hattermann, T., Hoffman, M. J., Humbert, A., Huybrechts, P., Jourdain, N. C., Kleiner, T., Larour, E., Leguy, G. R., Lowry, D. P., Little, C. M., Morlighem, M., Pattyn, F., Pelle, T., Price, S. F., Quiquet, A., Reese, R., Schlegel, N.-J., Shepherd, A., Simon, E., Smith, R. S., Straneo, F., Sun, S., Trusel, L. D., Van Breedam, J., van de Wal, R. S. W., Winkelmann, R., Zhao, C., Zhang, T., and Zwinger, T. (2020). ISMIP6 Antarctica: a multi-model ensemble of the Antarctic ice sheet evolution over the 21st century. *The Cryosphere*, 14, 3033–3070. https://doi.org/10.5194/tc-14-3033-2020

Shreve, R. (1972). Movement of water in glaciers. *Journal of Glaciology*, 11(62), 205-214. https://doi.org/10.3189/S002214300002219X

Tedesco, M., Lüthje, M., Steffen, K., Steiner, N., Fettweis, X., Willis, I., Bayou, N., and Banwell, A. (2012). Measurement and modeling of ablation of the bottom of supraglacial lakes in western Greenland. *Geophysical Research Letters*, 39, L02502. https://doi.org/10.1029/2011GL049882

Trusel, L. D., Frey, K. E., Das, S. B., Kuipers Munneke, P., and van den Broeke, M. R. (2013). Satellite-based estimates of Antarctic surface meltwater fluxes. *Geophysical Research Letters*, 40, 6148–6153. https://doi.org/10.1002/2013GL058138

van den Broeke, M. R., Enderlin, E. M., Howat, I. M., Kuipers Munneke, P., Noël, B. P. Y., van de Berg, W. J., van Meijgaard, E., and Wouters, B (2016). On the recent contribution of the Greenland ice sheet to sea level change. *The Cryosphere*, 10, 1933–1946. https://doi.org/10.5194/tc-10-1933-2016

van der Veen, C. J. (1998). Fracture mechanics approach to penetration of surface crevasses on glaciers. *Cold Regions Science and Technology*, 27(1), 31-47. https://doi.org/10.1016/S0165-232X(97)00022-0

van der Veen, C. J. (2007). Fracture propagation as means of rapidly transferring surface meltwater to the base of glaciers. *Geophysical Research Letters*, 34, L01501. https://doi.org/10.1029/2006GL028385

Vaughan, D. (1993). Relating the occurrence of crevasses to surface strain rates. *Journal of Glaciology*, 39(132), 255-266. https://doi.org/10.3189/S0022143000015926

Walder, J., and Fowler, A. (1994). Channelized subglacial drainage over a deformable bed. *Journal of Glaciology*, 40(134), 3-15. https://doi.org/10.3189/S0022143000003750

Wei, W., Blankenship, D. D., Greenbaum, J. S., Gourmelen, N., Dow, C. F., Richter, T. G., Greene, C. A., Young, D. A., Lee, S., Kim, T.-W., Lee, W. S., and Assmann, K. M. (2020). Getz Ice Shelf melt enhanced by freshwater discharge from beneath the West Antarctic Ice Sheet. *The Cryosphere*, 14, 1399–1408. https://doi.org/10.5194/tc-14-1399-2020

Werder, M. A., Hewitt, I. J., Schoof, C. G., and Flowers, G. E. (2013). Modeling channelized and distributed subglacial drainage in two dimensions. *Journal of Geophysical Research: Earth Surface*, 118(4), 2140–2158. https://doi.org/10.1002/jgrf.20146

Werder, M. A. (2016). The hydrology of subglacial overdeepenings: A new supercooling threshold formula. *Geophysical Research Letters*, 43(5), 2045–2052. https://doi.org/10.1002/2015GL067542

Yang, K., and L. C. Smith (2016). Internally drained catchments dominate supraglacial hydrology of the southwest Greenland Ice Sheet. *Journal of Geophysical Research: Earth Surface*, 121, 1891–1910. https://doi.org/10.1002/2016JF003927